INFORMATION TO USERS

This material was produced from a microfilm copy of the original document. While the most advanced technological means to photograph and reproduce this document have been used, the quality is heavily dependent upon the quality of the original submitted.

The following explanation of techniques is provided to help you understand markings or patterns which may appear on this reproduction.

1. The sign or "target" for pages apparently lacking from the document photographed is "Missing Page(s)". If it was possible to obtain the missing page(s) or section, they are spliced into the film along with adjacent pages. This may have necessitated cutting thru an image and duplicating adjacent pages to insure you complete continuity.

2. When an image on the film is obliterated with a large round black mark, it is an indication that the photographer suspected that the copy may have moved during exposure and thus cause a blurred image. You will find a good image of the page in the adjacent frame.

3. When a map, drawing or chart, etc., was part of the material being photographed the photographer followed a definite method in "sectioning" the material. It is customary to begin photoing at the upper left hand corner of a large sheet and to continue photoing from left to right in equal sections with a small overlap. If necessary, sectioning is continued again — beginning below the first row and continuing on until complete.

4. The majority of users indicate that the textual content is of greatest value, however, a somewhat higher quality reproduction could be made from "photographs" if essential to the understanding of the dissertation. Silver prints of "photographs" may be ordered at additional charge by writing the Order Department, giving the catalog number, title, author and specific pages you wish reproduced.

5. PLEASE NOTE: Some pages may have indistinct print. Filmed as received.

Xerox University Microfilms
300 North Zeeb Road
Ann Arbor, Michigan 48106

THE PHASE-NULL METHOD FOR AUTOMATIC DETERMINATION OF DOUBLE-LAYER CAPACITY

by

ROBERT SAUL SCHWARTZ

A dissertation submitted to the Graduate Faculty in Chemistry in partial fulfillment of the requirements for the degree of Doctor of Philosophy, The City University of New York.

1974

This manuscript has been read and accepted for the Graduate Faculty in Chemistry in satisfaction of the dissertation requirement for the degree of Doctor of Philosophy.

May 8, 1974
date

Joseph Gerstein
Chairman of Examining Committee

5/8/74
date

Leonard H. Schwartz
Executive Officer

Supervisory Committee

The City University of New York

To Shelley.

Acknowledgments

The author wishes to express his sincere appreciation to Professor Joseph Glickstein for suggesting the problem and for his continued interest and active participation throughout this research. Thanks are due also to Mr. Ottmar Safferling and Mr. Stanley Wacks for their invaluable technical assistance with this project.

Grateful acknowledgment is made to Brooklyn College for financial aid in the form of teaching assistantships and to the City University for financial aid in the form of research assistantship for the academic year 1971 - 72.

Table of Contents

List of Tables

List of Tables

List of Figures

Introduction

Double Layer Theory

Structure and Capacitance of the Double Layer

It is generally accepted that there exists at every material interface an array of charged particles and/or oriented dipoles generally referred to as an electrical double layer, or more simply a double layer. (1) In particular this is true at the boundary between an electrode, and the solution in which it is immersed. The double layer at the electrode-solution interface has been the subject of numerous investigations over the years.

The first quantitative theory was that of Helmholtz (2) and Quincke (3). It was assumed that the double layer acted as a capacitor of constant value. There existed, according to their ideas, two rigid sheets of equal but opposite charge, one on the electrode and the other in the solution, separated by a constant distance. This description is in precise geometrical analogy to an ordinary electrical capacitor.

The modern theory of the structure of the double layer, due mainly to the contributions of Gouy, Chapman, Stern, and Grahame (4, 5, 6, 7), holds that the interfacial region at the electrode-solution boundary contains at least three, and sometimes more, distinct subregions or layers; the name double layer persisting only through historical precedent. Proceeding outward from the electrode to the solution, the first layer or subregion is the electrode itself. If the electrode is metal, as is generally the case, the charge resides in so

thin a layer in the surface of the metal that it may be considered two-dimensional. Thus the metallic side of the double layer is the same in modern theory as it is in that of Helmholtz. However, the solution side of the interface has a more complicated structure. Here we find at least two regions, due to the two different types of forces which come into play. The first region, that closest to the electrode, and arising from short-range, chemical-type forces, is essentially two-dimensional in nature, and is called the inner layer. It consists of a monolayer of solvent molecules, (which if polar are oriented electrically with respect to the electrode) perhaps some neutral adsorbed molecules, and in solutions of electrolytes possibly some ions, generally anions, which have lost at least that part of their solvation sheaths closest to the electrode. These molecules and ions present in the inner layer are said to be specifically adsorbed, their centers forming the locus of the inner Helmholtz plane. The second region, called the diffuse layer, contains those ions which do not interact strongly enough with the electrode to lose part of their solvation sheaths, but are still subject to weaker long-range electrostatic forces. The structure of this region can be thought of as arising from the effect of coulombic ordering superimposed on thermal disordering. Ions attracted into this region are said to be non-specifically adsorbed, the locus of the centers of the closest approaching non-specifically adsorbed ions forming the outer Helmholtz plane. The diffuse layer extends from the outer Helmholtz plane to the bulk of the solution.

Although the precise geometrical analogy between an ideal electrical capacitor and the double layer has been invalidated, the concept of a capacitance associated with the double layer has remained. Indeed, the measurement of double-layer capacity has provided much of the detailed knowledge about the structure of the double layer. (1)

Charging Current

In the areas of electroanalytical chemistry and electrode kinetics, the double layer and its associated capacitance introduce complications which must be dealt with if accurate results are desired. One of these complications arises from the ability of the double layer to pass condenser or charging current under appropriate conditions. As a first approximation, the idea first put forward by Randles (8) may be invoked that the double-layer capacitance may be thought of as an electrical element in the equivalent circuit of a cell, which is connected in parallel with the faradaic impedance. Current will flow through the double layer if the voltage across it is changing, and/or its capacitance is changing as shown in the following equations.

The operational definition of a capacitor is:

$$C = \frac{q}{V} \qquad (1)$$

Here C is the capacitance, q is the magnitude of the charge on either plate and V is the voltage drop across the capacitor. Solving for q in equation (1) gives:

$$q = CV \qquad (2)$$

The current passing the capacitor may be found by differentiating equation (2) with respect to time:

$$\frac{dq}{dt} = C\frac{dV}{dt} + V\frac{dC}{dt} \qquad (3)$$

The instantaneous current, i, passing through any point in a circuit is:

$$i = \frac{dq}{dt} \tag{4}$$

Substituting equation (4) into equation (3), we obtain the expression for the current, i_c, through the capacitor:

$$i_c = C \frac{dV}{dt} + V \frac{dC}{dt} \tag{5}$$

At a dropping mercury electrode (DME) the term dC/dt is not zero due to the change in area of the electrode with time, the capacitance being directly proportional to the area. Thus, there will always be a charging current at the DME provided V is not zero. In addition, if a time-varying potential is employed, equation (5) predicts charging current due to the term dV/dt. The latter condition applies to all electrodes, and not just to the DME. This charging current adds to the faradaic current, due to the reaction occuring at the electrode, to produce the total cell current. It is this total cell current which is experimentally accessible. In order to measure the faradaic contribution only, which is the object in many electrochemical techniques, some provision must be made for correcting for charging current.

Integral and Differential Capacity

There are two problems which arise when one attempts to define double-layer capacity operationally in a manner analogous to equation (1). These are:

(1) The V term in equation (1) refers to the difference in potential between the two plates of a capacitor. Since the "plates" of the double layer consist of two different phases (solid electrode and liquid solution) the potential difference cannot be measured.

(2) The capacitance of the double layer is not constant, and depends in a complicated way on the electrode potential.

In order to get around the first problem we go back to equation (1), the operational definition of an ordinary electrical capacitor, and note that $q = 0$ when $V = 0$. Now there exists for any electrode dipping in a given solution a unique potential at which its surface charge density, q^m, is zero. This potential is called the electrocapillary maximum potential, and is denoted by the symbol E_z. If we measure the electrode potential, E, with respect to E_z we can define the double-layer capacity as:

$$K_o = \frac{q^m}{E^*} \qquad (6)$$

Here K_o is the specific integral capacity of the double layer (capacity per unit area) and E* is the electrode potential with respect to E_z. (Note that E and E_z are electrode potentials measured with respect to the same reference electrode.)

$$E^* = E - E_z \qquad (7)$$

The integral capacitance is important in d.c. techniques where charging current arises due to the term dC/dt in equa-

tion (5). The equation for charging current, i_c, in terms of K_o may be derived as follows:

If q is the charge on the electrode and A is its area, we have:

$$q = Aq^m \tag{8}$$

Substitution of equation (8) into equation (4) gives:

$$i_c = \frac{d(Aq^m)}{dt} \tag{9}$$

Since q^m is a function only of electrode potential and composition of the solution then:

$$i_c = q^m \frac{dA}{dt} \tag{10}$$

Solving q^m in equation (6) and substituting the result into equation (10)we obtain the following expression for charging current in a d.c. technique.

$$i_c = K_o E^* \frac{dA}{dt} \tag{11}$$

Thus we see that in a d.c. technique, charging current is directly proportional to the specific integral capacity. In a.c. techniques, however, the equation for charging current is modified due to the second problem mentioned, viz. the electrode capacity is a function of potential. The equation

for a.c. charging current may be derived as follows.

Solving for q^m in equation (6) and substituting the result into equation (9) we obtain:

$$i_c = \frac{d\ (A\ E^*\ K_o)}{dt} \tag{12}$$

Carrying out the differentiation:

$$i_c = A\ \frac{d\ (E^*K_o)}{dt} + K_oE^*\ \frac{dA}{dt} \tag{13}$$

The second term on the right is the d.c. charging current as can be seen by comparison with equation (11). Since we are now interested in the a.c. charging current, we will drop this term. The first term on the right is the a.c. charging current. Carrying out the indicated differentiation we obtain:

$$i_c = A\left[K_o\ \frac{dE}{dt} + E^*\ \frac{dK_o}{dt}\right] \tag{14}$$

Note that $dE^* = dE$, since E_z is a constant.

Now K_o is a function of time since it is a function of potential and the potential varies with time in an a.c. technique. The derivative of K_o with respect to time can be written as:

$$\frac{dK_o}{dt} = \frac{dK_o}{dE} \times \frac{dE}{dt} \tag{15}$$

Substituting this expression for dK_o/dt into equation (14) and rearranging gives:

$$i_c = \left[A\ (K_o + E^* \frac{dK_o}{dE})\right] \frac{dE}{dt} \qquad (16)$$

For an ordinary electrical capacitor whose capacity is independent of potential we have from equation (5) that:

$$i_c = C \frac{dV}{dt} \qquad (17)$$

By analogy with equation (17) we see that the term in brackets in equation (16) plays the same role as C in equation (17). This expression is called the differential capacitance, C_d, while the term in parenthesis is the specific differential capacitance, C_d^o. (Differential capacitance per unit area.) By differentiating equation (6) with respect to E it can be shown that:

$$C_d^o = \frac{dq^m}{dE} \qquad (18)$$

Now we may write equation (16) as:

$$i_c = C_d \frac{dE}{dt} \qquad (19)$$

Here i_c is the a.c. charging current due to the use of an a.c. voltage. Thus we see that the a.c. charging current is directly proportional to differential capacity. A.c. techniques thus measure differential capacity, whereas inspec-

tion of equation (11) shows that d.c. techniques measure integral capacity. Of the two kinds of capacitance, C_d is the more important. A. c. impedance bridge measurements of C_d, usually at a DME, have provided much of the knowledge of the structure of the double layer. (1) It has been noted by Mohilner (1) that C_d is a more useful parameter for investigating double-layer structure than is integral capacitance.

Double Layer Effects In Electrochemistry

Electrode Kinetics - The Frumkin Effect

In the study of electrode kinetics, one seeks to determine the rate of electron transfer in the electrode reaction as a function of concentration of electroactive material and potential of the electrode. In order to obtain the rate of electron transfer, one first measures the overall rate of reaction as evidenced by the total faradaic current and then corrects for the rate of mass transfer. Frumkin (9) realized that in order for electron transfer to occur, the electroactive species must first come as close to the electrode as possible, which in the case of non-specific adsorption is in the outer Helmholtz plane (O.H.P.). If this is so, then the rate of the reaction can be expressed as a function of the concentration of electroactive material in the O.H.P. One must, of course, use the correct effective potential difference as "seen" by the electroactive substance in the O.H.P. in the rate equations.

As it turns out, in order to calculate the concentration of a given ionic species in the O.H.P. and the effective potential difference, one must first determine ϕ, the potential in the O.H.P. This quantity can be calculated using the equations of the Gouy-Chapman-Stern theory of the diffuse layer. The starting point is the experimental determination of C_d at the potential of interest.

Adsorption

Another area where the determination of double-layer

capacity proves helpful is that of adsorption. The adsorption of electroinactive surfactants and that of electroactive material have a profound effect on double-layer capacity and viceversa. (10) Adsorption of electroinactive surfactants usually leads to large depressions in C_d and sometimes to sharp peaks too. (11) Electrode kinetics can be markedly affected by this type of adsorption also. (12) Specific adsorption of electroactive species can, in addition to altering C_d, significantly change characteristics of the faradaic impedance. (10) The presence and effects of specific and non-specific adsorption can be determined using measurements of C_d. (13)

Need for Determination of Double-Layer Capacity in the Presence of an Electrode Reaction

Practically all of the work thus far on the double layer and its effects has been done using ideal polarized electrodes, that is, in the absence of faradaic current. However, it is in the properties and effects of the double layer in the presence of faradaic current that electrochemists are most interested. For example, specific adsorption of electroactive species can greatly modify the double-layer capacity and thus the charging current, even in the presence of a large excess of base electrolyte. If the electroactive species is present in low concentration, large errors can be made in determining its concentration if usual methods of correcting for charging current are used. In this case, for accurate subtraction of charging current, the charging current must be determined in the test solution simultaneously with total cell current. In addition, unless the most stringent methods of purification of test solutions are used, one can never be sure that specifically adsorbed trace impurities are absent, thus affecting the capacity and hence the charging current in an unknown way. (14) Thus, the use of a dummy cell containing only base electrolyte to measure charging current is not a valid procedure for correcting for charging current. This is especially true in the case of trace analysis where charging current is a significant fraction of the total cell current.

The measurement of double-layer capacity in the presence of faradaic current can also tell us something about the mech-

anism of the electron-transfer reaction occuring at an electrode. For example, one might be able to determine whether or not specific adsorption of electroactive species, or perhaps even the product of the electrode reaction, played a role in the reaction mechanism. Specific adsorption of electroinactive material can also alter the kinetics of the faradaic reaction. The adsorbed material might, for example, inhibit the rate of electron transfer or even interact chemically with electroactive material at the electrode surface. (12)

It is clear from the foregoing discussion that determination of double-layer capacity in the presence of faradaic current is an important objective in electrochemical studies, and it is to this end that this research is directed.

Previous Methods of Measuring Double-Layer Capacity

Methods in the Absence of Faradaic Current

Theory - The Lippmann Equation

Most of the work to date on determination of double-layer capacity has been done on systems comprised of ideal polarized electrodes, usually mercury in contact with an aqueous solution of an inert (electroinactive) salt. An ideal polarized electrode is one which can be polarized without a concurrent transfer of charge across the electrode-solution interface. As Grahame (7) has pointed out, while no real electrode can behave exactly as an ideal polarized electrode over all ranges of potential, the behavior of a mercury electrode immersed in an aqueous solution of an electroinactive salt closely approximates this behavior over a wide range of potential.

There are three different classes of experiments which can be performed to determine the value of the double-layer capacity at an ideal polarized electrode. One can calculate the value of the double-layer capacity from electrocapillary curves, which are plots of surface tension versus potential. Another approach is to measure the surface charge as a function of potential, while the third, and most accurate method, is to determine the value of the double-layer capacity directly.

Surface tension, surface charge and double-layer capacity are related through the electrocapillary equation, sometimes referred to as the Lippmann equation, first derived by Lippman. (15) This equation states that a constant chemical

potential, μ, the rate of change of surface tension, σ, with respect to potential is equal to the negative of the surface charge density on the electrode. Mathematically, this statement becomes:

$$\left(\frac{\partial \sigma}{\partial E}\right)_{\mu} = -q^{m} \qquad (20)$$

Since the differential double-layer capacity is defined as the rate of change of surface charge density with respect to potential, it can be determined from electrocapillary curves by a double differentiation with respect to potential, or from curves of surface charge density versus potential by a single differentiation with respect to potential. Mathematically stated we have:

$$C_{d}^{o} = \left(\frac{\partial q^{m}}{\partial E}\right)_{\mu} = -\left(\frac{\partial^{2} \sigma}{\partial E^{2}}\right)_{\mu} \qquad (21)$$

From Surface Tension Measurements

The determination of double-layer capacity by measuring surface tension is fairly difficult. The measurements must be made with exceeding accuracy since a double differentiation must be performed. While there are many methods of measuring the surface tension of a mercury electrode in contact with an aqueous solution, the most accurate results are those in which the Lippmann capillary electrometer is employed, (16) This is the instrument invented by Lippmann (17) and used in his pioneering studies of the relationship between surface

tension and polarizing potential. The capillary electrometer consists of a mercury column ending in a fine tapering capillary tube which dips into the test solution. The mercury is polarized to a given potential and the height of the column is adjusted so that the mercury in the capillary tube comes to rest at a given point. From the height of the mercury column the surface tension can be calculated.

From Measurement of Surface Charge

The calculation of double-layer capacity by direct measurement of surface charge density as a function of potential requires the use of a dropping electrode. Again, for obvious reasons, mercury is the electrode material of choice. The method to be described was first initiated by Varley (18) and subsequently developed by Lippmann (15) as a means of checking results obtained from electrocapillary curves. It has since been used by various other investigators. (19, 20, 21)

Experimentally, one immerses a dropping mercury electrode into an aqueous solution of an electroinactive salt which has been scrupulously freed of all traces of electroactive impurities, including dissolved oxygen, and polarizes it to the potential of interest. As each drop grows a current must flow in order to charge the double layer to the desired potential. It is assumed that this charging process occurs much more rapidly than the rate of growth of the drop so that an equilibrium is always maintained. One then measures the amount of charge which has flowed into the mercury drop at a given time during drop life, usually drop fall, either

by integration of the charging current or by measuring the amount of charge carried away by the drop. The latter measurement may be accomplished by connecting the dropping mercury electrode to a mercury pool at the bottom of the cell by an external wire with a galvanometer in series. As a drop falls it carries with it a definite amount of electrical charge. When the drop strikes the mercury pool and coalesces into it, this charge flows back to the dropping electrode through the external wire and the galvanometer. Again, integration of the resulting current gives the amount of charge on the drop. The area of the drop can be calculated from a knowledge of its weight and by assuming the drop to have a spherical shape. The total charge divided by the area of the drop gives the surface charge density. Differentiation of the surface charge density with respect to potential yields the specific differential capacity, C_d^o.

Direct Measurement Methods

Direct measurements of double-layer capacity are based upon the idea that the double layer behaves as an ordinary electrical capacitor with respect to electrical signals. Thus, any method which can be used to determine the capacity of an ordinary electrical capacitor can be used to determine the capacity of the double layer. The only difference between the electrical behavior of the double layer and that of an electrical capacitor is that the capacity of the former is a function of potential, while that of the latter is not. As noted previously in this work and pointed out by Grahame

(22), this phenomenon has led to the definition of two types of capacity associated with the double layer, viz. static or integral capacity and differential capacity.

One approach to the measurement of differential capacity involves the use of charging curves. This technique, employed by various investigators (23, 24), involves the use of a constant d.c. current to polarize an electrode. Using the definition of differential capacity:

$$C_d = \frac{dq}{dE} \tag{22}$$

and substituting the expression for dq which can be derived from equation (4)

$$dq = i\ dt \tag{23}$$

we can write, after rearrangement,

$$C_d = \frac{i}{\frac{dE}{dt}} \tag{24}$$

Thus, one measures electrode potential as a function of time (charging curve), usually with an oscilloscope, and calculates the slope, dE/dt at the potential of interest. The current divided by the slope gives the differential capacity.

Other approaches to measurement of C_d involve the use of a small-amplitude, sine-wave voltage superimposed on the d.c. polarizing voltage. The most common, and perhaps the most accurate, technique utilizing this approach is the a.c.

bridge method. First used by Krüger (25) and brought to a high degree of perfection by Grahame (22, 26), it involves placing the electrolytic cell in one arm of an a.c. impedance bridge with a standard variable resistance and capacitance in series in another arm. The electrode at which the capacity is to be measured is polarized to the potential of interest and the variable resistance and capacitance are adjusted to bring the bridge unbalance voltage (a.c.) to zero. At this point, it can be shown that the value of the variable resistance and capacitance are equal to the cell resistance and differential double-layer capacity at the electrode of interest.

Other investigators have used small amplitude square waves (27), triangular waves (28), and voltage pulses (29) superimposed upon the d.c. polarizing potential to measure the double-layer capacity at ideal polarized electrodes.

Methods in the Presence of Faradaic Current

Introduction

Until recently the measurement of double-layer capacity in the presence of faradaic current had not been done. The experimental difficulty is due to the fact that only the total cell response to an electrical stimulus can be measured. In the presence of a faradaic reaction, the total response is due to both faradaic and double-layer (or non-faradaic) contributions. This difficulty may be clarified with the aid of a diagram representing the equivalent circuit for an electrolytic cell in the presence of a faradaic reaction.

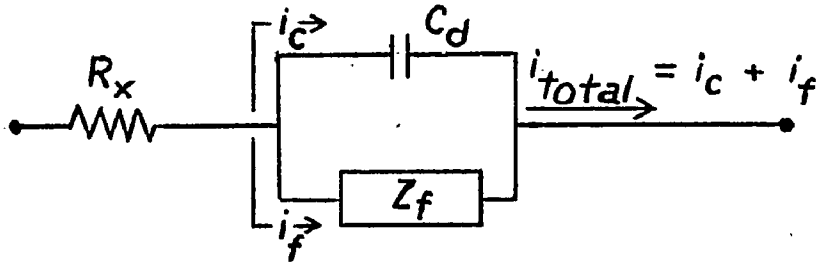

I

Here R_x is the series resistance due to contributions from the solution and electrodes, C_d is the double-layer capacity and Z_f is the faradaic impedance due to the electron transfer reaction. This picture of the equivalent cell circuit in the presence of a faradaic reaction is similar to the one first described by Randles. (30)

As can be seen from the above diagram, the faradaic and charging currents add to give the total cell current. It is the total cell current which is accessible experimentally. Thus, any method for measuring the double-layer capacity which involves the measurement of cell current due to a vol-

tage stimulus will not work in the presence of a faradaic reaction. If an a.c. impedance bridge is used, it will measure the total cell impedance which includes contributions from Z_f and C_d. In addition, surface tension methods are invalid since the Lippmann equation does not apply to charge-transfer electrodes. (1)

The Method of Sluyters-Rehbach

The first investigators to develop a technique capable of measuring double-layer capacity in the presence of faradaic current were Sluyters-Rehbach and Sluyters. (31) They employed the same a.c. impedance bridge technique as described previously, with a novel method of data treatment. They combined a.c. circuit theory for complex impedances with the familiar Randles equivalent circuit of impedance of an electrolytic cell. (30) These together with the equations for the faradaic impedance enabled them to derive expressions for the total cell impedance in terms of its real and imaginary parts. The latter are measured directly by the a.c. bridge technique being the equivalent series resistance and reactance, respectively, of the cell. By appropriate manipulation they were able to derive from these expressions an equation involving the real and imaginary parts of the cell impedance, the double-layer capacity, frequency of the applied a.c. signal, and a parameter which they designated as the irreversibility quotient which is related to the components of the faradaic impedance. The irreversibility quotient must be determined by performing a series of experiments at different concentrations or at different frequencies.

This leaves the double-layer capacitance as the only unknown.

While the Sluyters-Rehbach method represented a breakthrough in the field of electrochemistry, the need for performing several experiments and the extensive data manipulation required for the calculation of a single experimental point detracts somewhat from this approach. Since Sluyters-Rehbach's method first appeared, there have been other investigators (32, 33, 34) who have used similar techniques involving a.c. bridge measurements of total cell impedance together with calculations of one sort or another.

The Method of Butler and Meehan

Another approach was employed by Butler and Meehan (35) in which they utilized a d.c. technique based on the difference in time dependance between charging current and faradaic current. Experimentally, current-time curves are recorded on an oscilloscope and the total current multiplied by $t^{1/3}$, where t is the time in the life of the drop at which the current is measured, is plotted versus $t^{1/2}$ if the electrode reaction is reversible, or versus t, if it is irreversible. A straight line is obtained which is extrapolated to $t = 0$. From the intercept the value of q, the surface charge density, can be calculated. One must then differentiate q with respect to E to obtain C_d.

The accuracy of this method suffers from several factors. The extrapolation becomes more inaccurate as the amount of faradaic current increases. In addition, the accuracy of the extrapolation depends on finding the right function of time

that best linearizes the data. In the case of an electrode reaction intermediate between completely reversible and completely irreversible, this involves trial-and-error fitting of data which is at best a tedious procedure. The need for differentiating the data to get C_d also degrades the accuracy. Since this is a d.c. technique, it cannot be applied to solid electrodes.

Pulse Methods

Pulse methods involve the application of an electrical pulse to an electrolytic cell which is initially at electrochemical equilibrium and the subsequent measurement of the cell overvoltage versus time as it relaxes towards equilibrium. The pulse can be a current or galvanostatic pulse (36), a charge or coulostatic impulse (37), or a voltage or potentiostatic pulse. (38) It is possible by proper analysis of the data from these experiments to extract the value of the double-layer capacity in the presence of faradaic current. Kooijman (39) developed a new method of analysis of the data from these experiments which involved the use of numerical tables to ease the difficulty of handling the complex functions involved.

Other investigators have used double galvanostatic pulses (40), and galvanostatic pulse followed by coulostatic impulse (41, 42) to determine faradaic impedance and double-layer capacitance.

There are two drawbacks involved in the use of pulse methods. The accuracy of the readout is rather low since an

oscilloscope must be used to record the rapid, transient behavior of the cell as it relaxes towards equilibrium. In addition, since the cell must be at electrochemical equilibrium before the application of the pulse, both components of the redox couple must be present, preferably at a concentration such that the equilibrium potential is close to the half-wave potential. Such a situation is not encountered in electroanalysis where only one component of the redox couple is present. The presence of this second component might markedly change C_d. In work at solid electrodes, attainment of the equilibrium potential would involve the use of prohibitively high concentration of the oxidized form of the metal.

The Phase Null Method for Automatic Determination of Double-Layer Capacity

Introductory Remarks

It is the purpose of the method developed in this thesis to introduce a novel way for automatically determining double-layer capacity. By suitable arrangement of experimental conditions it will be shown possible by means of the method described to accomplish this during the simultaneous flow of faradaic current. To the author's knowledge this has not been done before.

Theoretical Development

The Equivalent Cell Circuit

It is common practice in electrochemistry to describe the response of an electrolytic cell to electrical signals in terms of the "equivalent circuit" of the cell. This equivalent circuit is an imaginary network of simple electronic elements such as resistors and capacitors which would give the same response to the electrical stimulus as the actual cell does.

The simplest and most commonly accepted equivalent circuit for response to a.c. signals was first described by Randles in 1947 (30). This is shown in the following diagram.

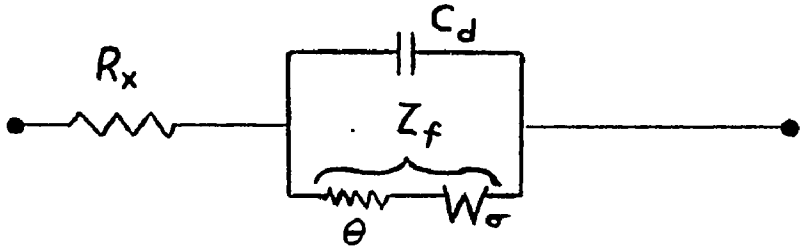

II

Here R_x and C_d are as previously described (fig. I., p. 18) while θ and W_σ constitute the elements of the faradaic impedance at the surface of the working electrode. One side of this parallel circuit represents the solution just adjacent to the electrode, while the other side is the electrode. This parallel connection is due to the fact that two separate processes are available to carry a.c. current, viz. double-layer charging and the faradaic process. Charging current flows through R_x and Z_f.

The Faradaic Impedance

Charge-Transfer Resistance

The charge-transfer resistance, θ, is due to the finite rate of electron transfer and behaves as a pure resistance. It is inversely proportional to both the rate constant, k_{sh}, for electron transfer and to the concentration of electroactive material. It depends exponentially upon the applied d.c. voltage, but is independent of the frequency of the a.c. voltage.

The Warburg Impedance

The Warburg impedance, W_σ, is due to the finite rate of mass transfer of electroactive material up to the electrode surface from the bulk of solution. It is a complex quantity which behaves as a resistance and capacitance of equal impedance connected in series. Its absolute value, $|W_\sigma|$, is given by

$$|W_\sigma| = \left[\sqrt{\frac{2}{\omega}}\right] \sigma \qquad (25)$$

where $\omega = 2\pi f$, f being the frequency of the applied a.c. voltage, and σ is a quantity which is inversely proportional to concentration, depends exponentially upon the applied d.c. voltage and the diffusion coefficients of the electroactive species.

Description of the Phase-Null Method

By judicious choice of experimental conditions, it is possible to arrange it so that the faradaic impedance becomes much

larger than the double-layer impedance, Z_{C_d}. When this condition is fulfilled, all but a negligible portion of the a.c. current will flow through the double layer. In other words, the double layer effectively shunts the faradaic impedance so that the equivalent circuit closely approximates that shown below.

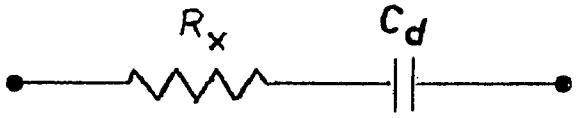

III

When this approximation is valid, the double-layer capacity can be determined by connecting the cell to the input of an operational amplifier, O.A., with a series R - C circuit in its feedback loop.

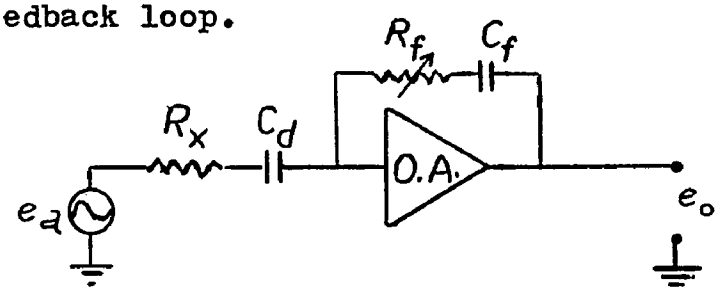

IV

Here e_a is the applied a.c. voltage, R_f is an adjustable feedback resistor, C_f is the feedback capacitor and e_o is the a.c. output voltage of O.A. (the operational amplifier.) If R_f is adjusted so that the phase angle of the feedback impedance matches that of the cell input impedance, a condition referred to as phase null in this work, it can be shown that the magnitude of the a.c. gain, G, of the amplifier (where G is defined as the magnitude of the ratio e_o/e_a) becomes equal to the ratio of double-layer capacity to feedback capacity. (See appendix A-1 for the derivation.) Thus, we have

$$G_o = \frac{C_d}{C_f} \qquad (26)$$

where G_o is the magnitude of the a.c. gain at phase null. (Note that, due to the fact that the amplifier is in the inverting configuration, e_o and e_a are exactly 180° out of phase at phase null. See any of the references 10, 43, 44, or 45 for background material on operational amplifiers.) Thus, once phase null is established, the determination of C_d becomes a simple matter.

It should be noted at this point that experimental conditions caused the response of the O.A. to differ somewhat from that predicted by equation (26). The sources of deviation are identified later in this section and a quantitative discussion is given in section V.

In practice the phase null is maintained automatically by a servo in which R_f is a photoconductive cell whose resistance depends on the light output of a lamp shining on it. The light output of the lamp in turn is made to depend on the difference between the phase of e_o and e_a, the "phase error signal." (The phase inversion due to O.A. is taken into account here.) This phase error signal drives the system to a phase null in precisely the same manner as an amplitude error signal drives a recorder to an amplitude-null. In both cases the error signal is reduced by the feedback arrangement to a negligibly small value.

A simplified diagram of this arrangement is shown below in figure V. The two blocks following the output of the O.A. and

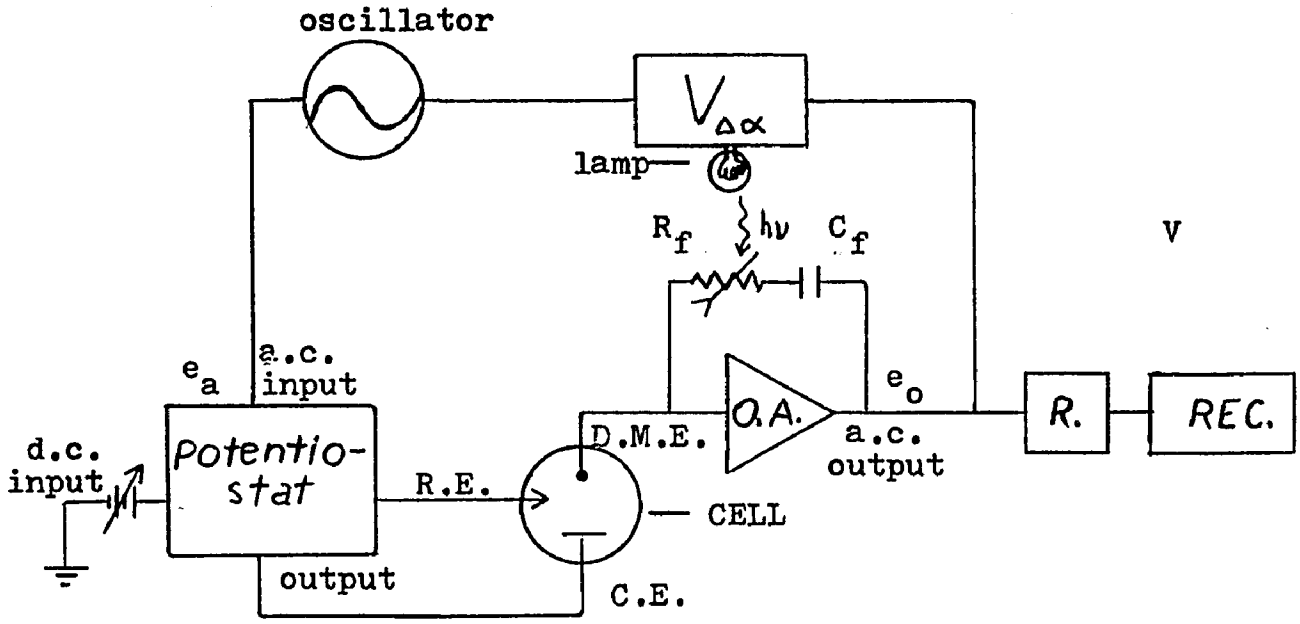

labelled R. and Rec. respectively, stand for a rectifier and recorder arrangement for the recording of the magnitude of the a.c. output, e_o, of the O.A. The block labelled $V_{\Delta\alpha}$ is a device which compares the phase of the applied a.c. voltage, e_a, with that of the output of the O.A., e_o, and produces an output voltage to drive the lamp which is dependent on this phase difference, $\Delta\alpha$. The cell is shown encircled, R.E. is the reference electrode, and C.E. is the counter electrode (anode). The potentiostat maintains the voltage of the D.M.E. with respect to R.E. equal to the sum of the a.c. and d.c. input voltages.

Conditions Under Which the Faradaic Impedance May Be Neglected

At High Frequency of the Applied A. C. Voltage

The double-layer impedance, Z_{C_d}, is given by

$$Z_{C_d} = \frac{1}{\omega C_d} \tag{27}$$

and thus decreases inversely with frequency.

The faradaic impedance, Z_f, is due to the sum of θ and W_σ. As has been noted earlier in this section, θ is independent of frequency while W_σ is inversely proportional to the square root of frequency. Thus as frequency is increased, Z_f approaches the limiting value of θ, while Z_{C_d} approaches zero.

$$\lim_{\omega \longrightarrow \infty} Z_f = \theta \tag{28a}$$

$$\lim_{\omega \longrightarrow \infty} Z_{C_d} = 0 \tag{28b}$$

Moreover, Z_f approaches its limit more slowly (as $\omega^{\frac{1}{2}}$) than does Z_{C_d} (as ω). Thus, for any electrode reaction it must be true that at sufficiently high frequency $Z_f \gg Z_{C_d}$. For slow reactions, where k_{sh} is small and θ is therefore large, Z_f will reach its lower limit at relatively low frequencies, and will remain large as ω is increased. In this case $Z_f \gg Z_{C_d}$ is true even at low frequencies. For fast reactions where k_{sh} is large and θ therefore is small, it will

be necessary to go to much higher frequencies to make the approximation valid.

At Low Concentration of Electroactive Material

Since Z_f is inversely proportional to concentration, lowering the concentration will increase Z_f and thus make the approximation that $Z_f \gg Z_{C_d}$ become more valid. When the concentration equals zero, as in supporting electrolyte solution, Z_f is infinite and the equivalent circuit in figure III would be an exact description instead of an approximation.

At D.C. Potentials Removed From $E_{\frac{1}{2}}$

To a good approximation, the faradaic impedance increases exponentially as a function of $\left|E-E_{\frac{1}{2}}\right|$, where E is the electrode potential and $E_{\frac{1}{2}}$ is the half-wave potential of the electroactive material. Thus, when the electrode potential is sufficiently removed from $E_{\frac{1}{2}}$, it will be true that $Z_f \gg Z_{C_d}$.

Experimental Conditions Causing Deviation From the Predicted Response

There are several factors which lead to the modification of the simple equation for the a.c. gain given previously. (Equation 26) The circuit used in the feedback loop (see figure IV) contained an additional resistance which shunted R_f and C_f.

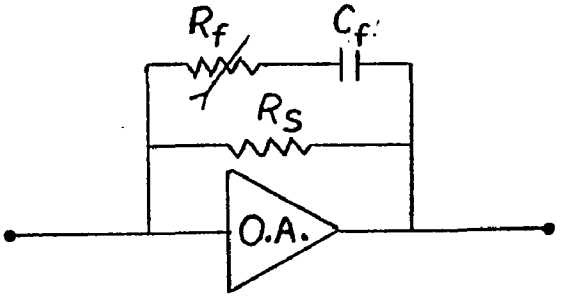

VI

Rs, the shunting resistance, is necessary to pass d.c. current due to the faradaic reaction.

In addition, it cannot be assumed that a perfect phase null is maintained at all times. The feedback control used to maintain the phase null implies the existence of a phase error signal, $\Delta\alpha$, which would certainly modify equation (26) which is valid only when $\Delta\alpha$ is zero.

The third factor leading to a non-ideal response has already been mentioned, viz. significant faradaic current.

As will be shown in later sections, the magnitude of the effects due to shunting and phase shift are rather small, leading to, at most, one or two per cent deviations from the response predicted by equation (26). In addition, the method of calibration employed gave good compensation for these effects. (See Section IV, E, 1; "Calibration of Electronics".) The magnitude of the error arising from the presence of faradaic current will be discussed in section V.

Experimental Methods

Electronics

Description of Operation and Circuit Diagram

The instrumentation described in this section is based on the extensive use of operational amplifiers. Excellent discussions of the theory and application of operational amplifiers in electrochemistry are given by Smith (10), Reilly (43), Booman and Holbrook (44) and Schwarz and Shain (45). The circuit diagram of the instrument is shown in figure 1, with a detailed diagram of the block labelled "Phase Detector" shown in figure 2. Specifications of components are listed in appendix A-4.

Amplifiers A-1, A-2 and A-3 form a potentiostat-current-amplifier section similar to that described by Smith (10). The network R-8, C-1 at the output of A-1 has been added for stabilization. The a.c. input to the potentiostat is derived by attenuating the bridge voltage of the General Radio Impedance Comparator with R-1 and R-2. The d.c. input voltage is derived by attenuating the -15 volt side of the amplifier power supply with R-4 and R-5. With this type of configuration, the potential of the DME with respect to the reference electrode is maintained at a value defined entirely by the potentiostat input voltages and the resistors R-1 through R-7, and is, thus, independent of the characteristics of the cell.

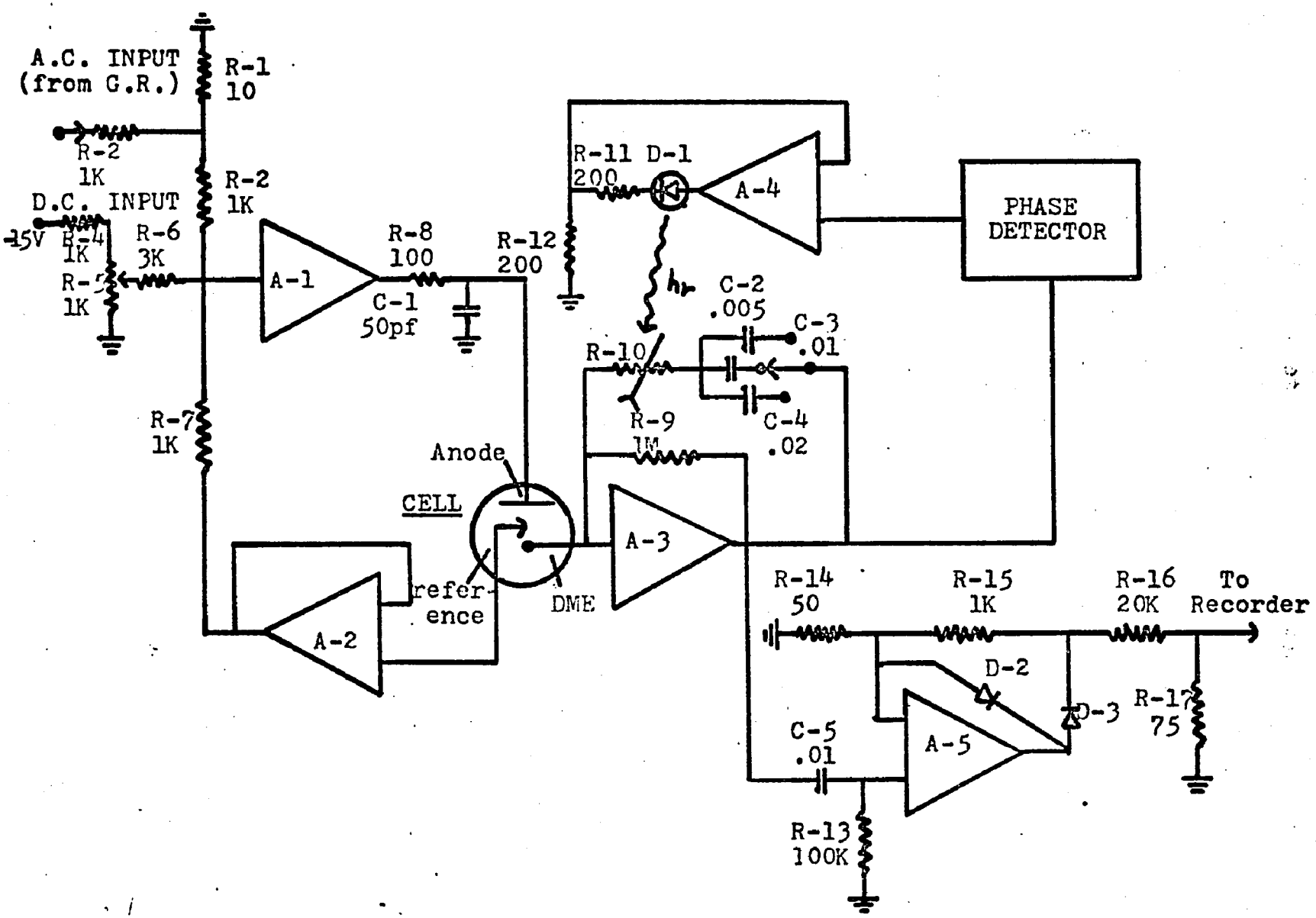

Figure 1. Circuit Diagram of Complete Instrument

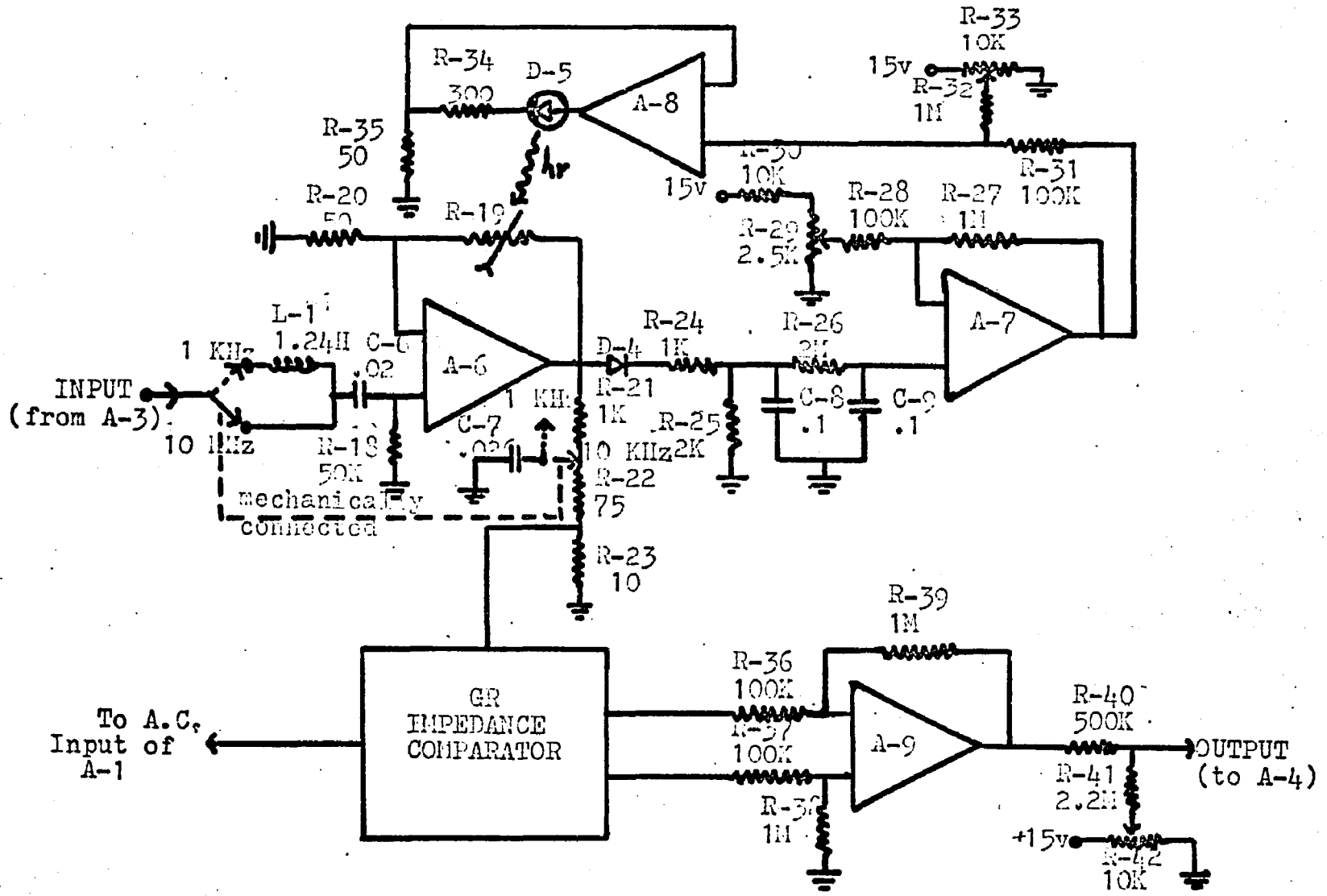

Figure 2. Circuit Diagram of Phase Detector

The cell current, which contains a.c. and d.c. components, flows into the input of the current amplifier, A-3, and through the feedback network consisting of R-9 in parallel with a series connection of R-10 and one of the range capacitors C-2, C-3 or C-4. R-9 provides a relatively low impedance path for the d.c. component of the cell current, while R-10 in series with one of the range capacitors provides a low impedance path for the a.c. component. Thus, practically all of the a.c. component of the cell current flows through R-10 in series with either C-2, C-3 or C-4. R-10 is a photocell whose resistance depends on the magnitude of the light output of the light-emitting diode (LED), D-1. The light output of D-1 depends ultimately on the difference in phase between the negative of the a.c. output of A-3 and the a.c. input voltage to the cell-the latter measured as the a.c. voltage appearing between the reference electrode and the DME. If this light output is properly phased, the resistance of R-10 will be driven to assume a value such that the phase of the a.c. output voltage of A-3 approaches that of the a.c. cell input voltage plus 180^{o}. (Since A-3 is an inverting amplifier, a perfect phase-null condition-where the phase angle of the cell impedance matches that of the feedback impedance of A-3 - would produce an output voltage exactly 180^{o} out of phase with the cell input voltage). The higher the gain of the phase-null feedback loop (the weries connection of the Phase Detector and the LED driver amplifier, A-4,) the more closely will the a.c. output of A-3 be 180^{o} out of phase with the a.c. cell input voltage. In the present case, this condition was achieved to better than 0.3^{o}.

The block labelled Phase Detector in figure 1 is shown in detail in figure 2. The function of the phase detector is to sense the phase difference between the negative of the a.c. output of A-3 and the a.c. cell input voltage, and produce an output voltage dependent on this phase difference. The input stage of the phase detector consisted of an automatic-gain-control (AGC) section involving amplifiers A-6, A-7 and A-8. The function of this section is to provide a pure a.c. output voltage of constant magnitude, exactly in phase with the a.c. output of A-3. The heart of this unit consists of amplifier A-6 with its feedback loop consisting of resistors R-19 and R-20. A-6 is connected as a non-inverting amplifier with gain. It may be shown that the gain, G, of A-6, referred to the signal at its positive input (junction of C-6 and R-18), is given by

$$G = 1 + R\text{-}19/R\text{-}20 \qquad (29)$$

In order to provide a signal of constant amplitude at the output of A-6, the gain of A-6 was made to vary inversely as the amplitude of the input signal from A-3, so that the product of the gain of A-6 and the amplitude of the input signal from A-3 remained constant. This was accomplished automatically by a servo system which controlled the resistance of R-19, a photoconductive cell, by means of the light output from a light-emitting diode, D-5. The signal used to drive D-5 was derived as follows. The output of A-6 was rectified by diode D-4, and

filtered by the network consisting of R-24, R-25, R-26, C-8 and C-9. This provided a d.c. voltage at the positive input of A-7 proportional to the magnitude of the output of A-6. A-7 compared this voltage with a reference voltage, e_r - derived by attenuating the +15 volt side of the amplifier power supply with the divider network consisting of R-29 and R-30 - and provided a voltage output directly related to their difference. If e_i is the input signal from the filter, and e_r is the voltage at the junction of R-28 and R-29, it may be shown that the output voltage of A-7, e_{A-7}, is given by

$$e_{A-7} = e_i \ (1+R\text{-}27/R\text{-}28) - e_r \ (R\text{-}27/R\text{-}28) \qquad (30)$$

Thus, the output of A-7 becomes more positive as e_i increases, and more negative as e_i decreases. The output of A-7 is divided by the network R-31 and R-32, and added to an offset voltage, e_{off}, (derived by attenuating the +15 volt side of the amplifier power supply with the potentiometer, R-33) to provide an input voltage, e_{A-8}, to the lamp driver amplifier, A-8 given by

$$e_{A-8} = e_{A-7} \left[R\text{-}32/(R\text{-}31+R\text{-}32)\right] + e_{off} \left[R\text{-}31/(R\text{-}31+R\text{-}32)\right] \qquad (31)$$

The lamp driver converts this input voltage to a current, i_L, to drive the lamp. The magnitude of this current is

$$i_L = \frac{e_{A-8}}{R\text{-}35} \qquad (32)$$

In operation, when the input to A-6 changes, the output of A-6 will start to change also. For arguments sake, let us say there is an increase in the magnitude of the a.c. input voltage to A-6. Now, the output of A-6 will start to increase. This will lead to an increase in e_i which leads, ultimately, to an increase in i_L. This means that the lamp will grow brighter causing the resistance of R-19 to decrease. This causes the gain of A-6 to decrease, thus tending to cancel the effect of the increase in input voltage. A similar argument may be applied when the input voltage decreases.

The series connection of C-6 and R-18 at the positive input of A-6 is a high-pass filter which blocks the d.c. component of the output voltage of A-3 and allows the a.c. component to pass. In order to compensate for the phase shift caused by the high-pass filter, it was necessary to introduce the phase correction components L-1 and C-7, so that the output of the AGC (junction of R-22 and R-23) was in-phase with, the output of A-3. L-1 was for phase compensation at 1 KHz, while C-7 provided compensation at 10 KHz. A double-pole, double-throw switch enabled one component to be switched in at the same time that the other component was switched out.

The output of the AGC is fed to the input of the General Radio Impedance Comparator. (A detailed description of this instrument is given in the instruction manual for the type 1605-A, -AH Impedance Comparator put out by the General Radio Company, West Concord, Massachusetts.) The comparator functions

as a phase-sensitive detector and provides d.c. output voltages proportional to the in-phase and quadrature components of the input signal, $E_I \angle\theta$, as shown below. (Note that the

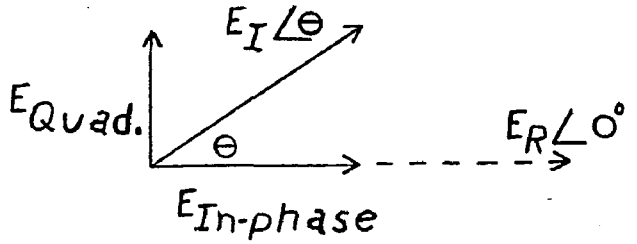

VII

comparator's bridge voltage, $E_R \angle 0°$, is used as a phase reference for this process. However, since $E_R \angle 0°$ is used to provide the a.c. input to the potentiostat, the correct phase reference is maintained.) Examination of diagram VII shows that the quadrature component is given by

$$E_{Quad.} = \left| E_I \angle\theta \right| \sin\theta \qquad (33)$$

where $\left| E_I \angle\theta \right|$ is the magnitude of the a.c. input to the comparator, and θ is the phase angle of E_I with respect to E_R. Since $E_I \angle\theta$ was held constant by the AGC, $E_{Quad.}$ is a function of $\sin\theta$ only. Thus, by taking $E_{Quad.}$ as the output of the comparator, a signal depending only on the phase shift between the a.c. output of A-3 and the a.c. cell input voltage was obtained. (The fact that A-3 is an inverting amplifier causes no problem since only a sign change is involved.)

Amplifier A-9 was connected as a difference amplifier and served as the output stage of the phase-detector unit. Since the output of the impedance comparator was a differential voltage of about 0.6 volts per degree of phase shift,

with a common mode voltage of about +40 volts, it was necessary to use a difference amplifier in order to reject the common mode voltage and provide a single ended output for proper operation of the LED driver, A-4. In addition, A-9 provided a voltage gain of ten which was necessary to provide the proper degree of open-loop gain for operation of the phase-null servo. The output voltage of the phase detector, e_{PD}, was obtained by attenuating the output voltage of A-9 using resistors R-40 and R-41, and adding an offset voltage derived by attenuating the +15 volt side of the amplifier power supply with potentiometer R-42.

In practice the operation of the phase-null servo may be illustrated as follows. Suppose the phase of the output of A-3 starts to lag the phase of the a.c. cell input voltage plus 180°. This would indicate that the phase angle of the feedback loop of A-3 was too negative and that the resistance of R-10 should be increased to retain a phase null. The phase detector senses this phase shift from the null point, and provides a d.c. output voltage dependent on this shift. In the present case of a phase-lag, the output of the phase detector would decrease. This decrease in the output of the phase detector causes the output of A-4 to decrease, thus lowering the light output of the light-emitting diode, D-1. This causes the resistance of R-10 to increase, thus tending to preserve the phase null. A similar argument may be employed if the phase shift were a lead instead of a lag.

Since the amplitude of the a.c. output of A-3 provides the desired indication of double-layer capacity, the instrument readout was obtained by recording the rectified a.c. output of A-3 on a stripchart recorder. Amplifier A-5 served as a precision half-wave rectifier. This is a standard circuit which is described in various sources (10, 46). The input circuit to A-5, consisting of C-5 and R-13 in series, is a high-pass filter to block the d.c. component of the output of A-3. The output of A-5 is attenuated by R-16 and R-17 and is then sent to the stripchart recorder.

Operating Points

A. C. Input Voltage

The a.c. input voltage of the DME with respect to the reference electrode was limited to between five and ten millivolts peak-to-peak. This is necessary to insure sufficient accuracy in the determination of C_d as has been noted by Grahame (22).

Photocell Range

The photocell must be made to operate in a region where it has the greatest sensitivity and smallest response time to changes in light level from the lamp. Since the photocell responds most rapidly at high light level and is most sensitive at low light level, a tradeoff was made in terms of response speed versus sensitivity wherein the photocell was made to operate over only a two-fold range of resistance values chosen in the best part of its operating region. (About 2.5 KΩ to 5.0 KΩ)

In order to achieve phase null over all C_d values encountered and at the same time maintain R_f within a limited range of values, it was necessary to use three different capacitors for C_f, each capacitor being used over a certain range of C_d values. It was found convenient to have these capacitors, C_{f_1} - C_{f_3}, in the ratio $2\ C_{f_1} = C_{f_2} = C_{f_3}/2$. Since the gain of the current amplifier at phase null is approximately C_d/C_f, a full scale response with C_{f_1}, can be made to read half scale by switching in C_{f_2}, etc. It was found in practice that the recorder could be made to record responses between half and full scale only, simply by switching to a different feedback capacitor. This enhanced the accuracy of the readout from the recorder chart.

Solutions and Chemicals

The water used in the preparation of all solutions was doubly distilled, with the second distillation carried out in a quartz still from dilute alkaline permanganate. The chemicals used, with the exception of thallium nitrate which was from Alpha Inorganics and labelled ultrapure, were all Baker Analyzed Reagent Grade. It was found that further purification was not necessary. The mercury used for the dropping mercury electrode as well as the calomel reference electrode was Bethlehem instrument grade and was prepared by continuous triple vacuum distillation and was guaranteed as having less than one part in 10^7 residue on evaporation of 2000 g. The gas used for deaerating the cell solution was helium of 99.995% purity from Matheson. The gas line was constructed of stain-

less steel, teflon and borosilicate glass. The helium was saturated with water vapor at 25.0° C by passing through a scrubbing tower filled with the doubly distilled water mentioned above, the bubbling tower being immersed in the 25.0°C water bath, and sent by way of a three way stopoock (borosilicate glass and teflon) either through or over the solution.

Cell and Electrodes

Cell

A diagram of the cell and electrodes used in this work is shown in figure 3. The cell was constructed of borosilicate glass and had a teflon stopcock. Four female ⌀ 12/18 joints on the top of the cell provided access for the three electrodes and a gas bubbler for deaeration. The latter was drawn down piece of glass tubing having an I.D. of about 0.5 mm at its tip. A fifth opening provided an inlet port for passing the stream of deaerating gas over the surface of the solution to provide an oxygen-free atmosphere while measurements were being taken. A water jacket was sealed onto the cell through which water at 25.0 ± 0.1°C was circulated during the experiments. The water was pumped from a water bath whose temperature was controlled by a YSI Proportional Temperature Controller. A teflon stopcock at the bottom of the cell permitted the mercury which accumulated from the D.M.E. to be withdrawn periodically for flow rate measurements during the course of an experiment.

The dimensions of the cell are as follows:

Outer diameter - 6.5 cm

Inner diameter - 4.5 cm

Cell height (bottom of water jacket to top of cell) - 11 cm

Height of water jacket - 8 cm

Active cell volume - 60 ml

Figure 3. Diagram of Cell

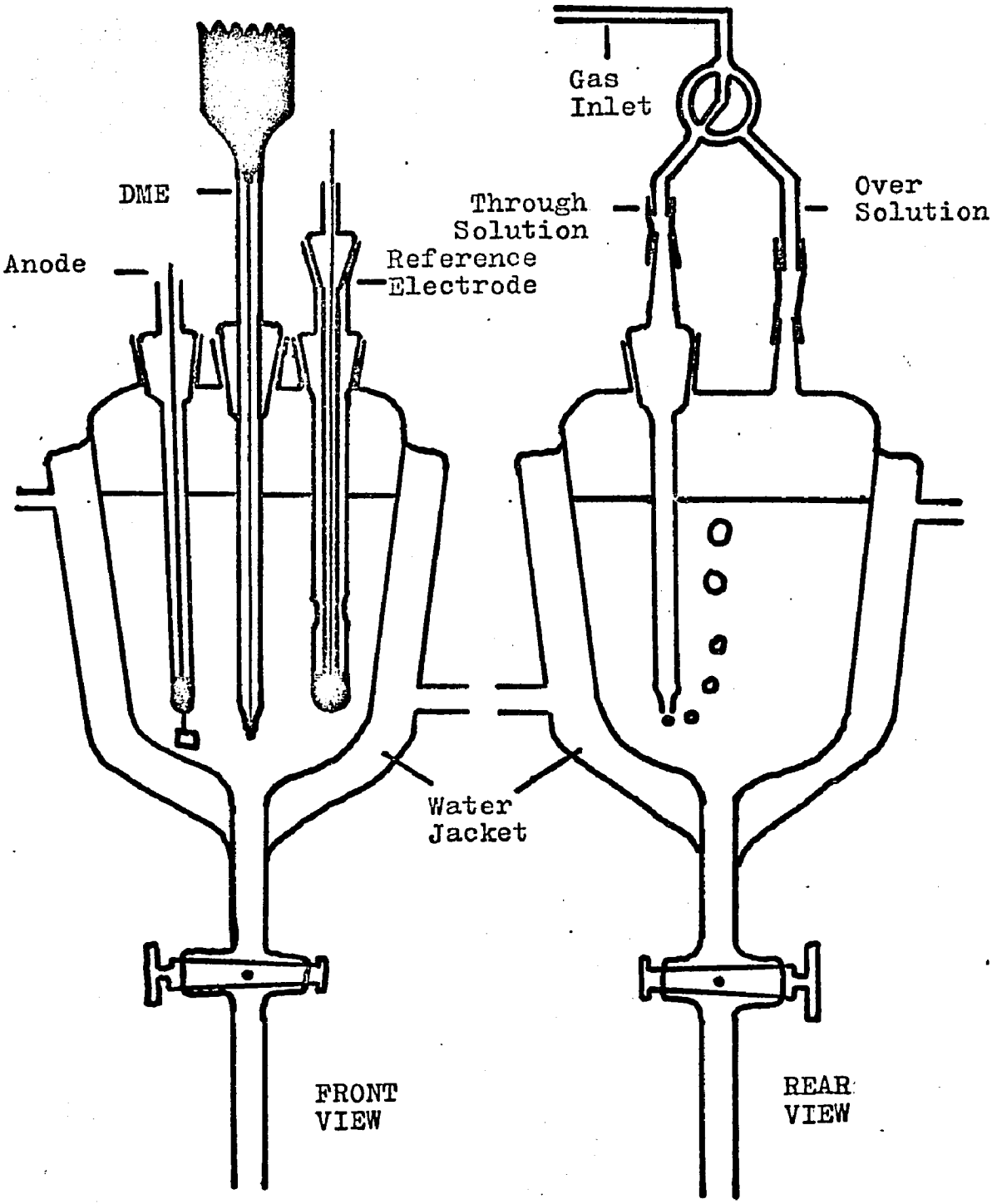

Electrodes

D.M.E.

The D.M.E. consisted of a capillary (Wilmad Glass Co., Buena, N. J.) fused onto a 50 ml. measuring pipet which served as the reservoir. The whole assembly was of borosilicate glass. The capillary as obtained had a uniform bore of 0.003 inches. A short section at the tip was drawn down to produce a bore of about 0.0015 inches and 0.5 cm. of this section was retained. The remainder of the capillary consisted of about 20 cm. of the original 0.003 inch bore tubing. Electrical contact with the mercury was made through the top of the reservoir with a piece of platinum wire. The D.M.E. was made to fit snugly into the ☎ 12/18 cell joint with an adaptor made from a piece of teflon rod.

The D.M.E., constructed in this manner, had a flow rate of about 0.94 mg. of mercury per second with a 30 cm. head of mercury. The drop time in deaerated 1 M KCl on open circuit was about 6.1 seconds.

Anode

The anode was constructed by fusing a piece of platinum, about 3 mm x 3 mm, into a piece of borosilicate glass tubing. The top of the tubing had a ☎ 12/18 male joint for insertion into the cell. Electrical contact was made with the anode by partly filling the glass tubing with mercury and inserting a copper wire.

Reference Electrode

Preparation

All the reference electrodes used in this work were of the calomel type with the electrolyte being the same as that used in the experiment. The electrode was constructed from a piece of borosilicate glass tubing, closed at one end with a male ⅋ 12/18 joint at the other end for insertion into the cell. Two holes about 1.5 cm from the bottom and about 2 mm in diameter provided electrical contact with the solution in the cell. Electrical contact with the electrode was made by inserting a piece of glass tubing with a piece of platinum wire fused into it. The tubing was filled with Woods metal which was melted, copper wire was inserted and the assembly allowed to cool. This tubing was provided with a one-hole rubber stopper which allowed for a tight fit between the electrode proper and the contact assembly.

The electrode was assembled by introducing a globule of mercury into the bottom of the electrode. The contact assembly was then inserted so that the platinum wire was below the mercury surface. Mercury and calomel were then shaken together and a small portion of the grayish scum that formed on the surface was transferred to the top of the mercury surface in the electrode through one of the holes provided for solution contact. This scum upon contact with the mercury spread out to cover the entire surface of the mercury with a pearly-gray film. The electrode was then filled with base electrolyte to be used in the experiment which had been deaerated so that the holes in the electrode were completely covered. This method is similar to one described by Hills and Ives (47).

Calibration

Before each run, a fresh reference electrode was assembled as described in the proceding section. The electrode was then calibrated by comparison with a commercial saturated calomel electrode of the cracked junction type (Leeds and Northrup). Three commercial electrodes were intercompared and the electrode having the median potential was chosen as the standard. The three saturated calomel electrodes always agreed with each other to better than one millivolt.

The reference electrode and the standard S.C.E. were placed in a 180-ml. tall-form beaker containing deaerated base electrolyte. The temperature was maintained at 25.0 ± 0.1°C. The potential of the cell was measured when it had reached a steady value. This procedure was repeated at the completion of each run. The drift in potential thus noted was always less than one millivolt.

In this work, all potentials are quoted with respect to the saturated calomel electrode chosen as described above. When reference is made to literature values of double-layer capacitance the potential is always with respect to the saturated calomel electrode. This sometimes required that the original potentials noted in the literature which were often measured with respect to other reference electrodes, such as the N.C.E. and 0.1 N.C.E., be shifted by the difference between the potential of the S.C.E. and that of the electrode used. Literature values (48) were used for these differences.

Procedures

Calibration of Electronics

As has been mentioned in section III of this thesis, the response of the instrument will deviate somewhat from that predicted by Equation 26 due to the effects of the shunting resistor, R_s, and the phase error signal, $\Delta\alpha$. The complete equation for the a.c. gain of the current amplifier, G, including the effects of shunting and phase error is (see derivation in appendix A-2)

$$G = \frac{C_d}{C_f}\left[1 + \frac{\sin\Delta\alpha}{\tan\alpha_f} - 2r\right] \qquad (34)$$

Here, α_f is the phase angle of the current amplifier feedback impedance and r is the ratio R_f/R_s. The term $\sin\Delta\alpha/\tan\alpha_f$ is the fractional change in response from Equation 26 due to the presence of a finite phase error signal ($\Delta\alpha \neq 0$) The term 2r is the fractional change due to the presence of the shunting resistor.

The magnitude of the term involving α is fairly small though it varies with frequency and double-layer capacity. An upper limit for this quantity may be estimated as follows. The phase null between the a.c. output of the current amplifier and the a.c. input voltage was monitored continuously during calibration and experimental runs using a Lissajous figure displayed on an oscilloscope. It was estimated that the minimum phase error signal that could be detected in

this manner amounted to approximately 0.3°. Since no detectable opening of the Lissajous figure - a straight line for two signals when they are either in phase or 180° out of phase - was observed, it can be assumed that $\Delta\alpha$ was at most 0.3°. The term tan α_f will cause the phase error term to be largest when it is smallest, since it appears in the denominator. This will occur at high values of frequency and double-layer capacity. Assuming values of 10 KHz and 1 μf for the highest frequency and double-layer capacity respectively, it turns out that tan $\alpha_f \cong 0.3$ as a lower limit. Inserting these values for tan α_f and $\Delta\alpha$ into the phase error term a value of 0.02 is obtained as an upper limit. Thus, the deviation from Equation 26 will be at most two per cent due to phase error.

The deviation due to the shunting effect is easily calculated by first noting that R_f, the photocell resistance, varied between 2.5 and 5.0 kilohms as has been mentioned in the section on operating points. Since the shunting resistor, R_s, had a value of 1 megohm, the term 2r varied between 0.005 and 0.01 leading to, at most, a one per cent deviation from Equation 26. Thus, due to the effects of phase error and shunting, the equation for the a.c. gain of the current amplifier is modified to the following form,

$$G = \frac{C_d}{C_f} \left[1 + \delta\right] \qquad (35)$$

where δ represents the combined effects of phase error and shunting and can vary from 0 to ± .02.

In order to provide compensation for the effect of δ, it was decided to calibrate the instrument using a simulated cell circuit which contained a standard, variable capacitor to represent C_d. This arrangement is shown below in diagram VIII.

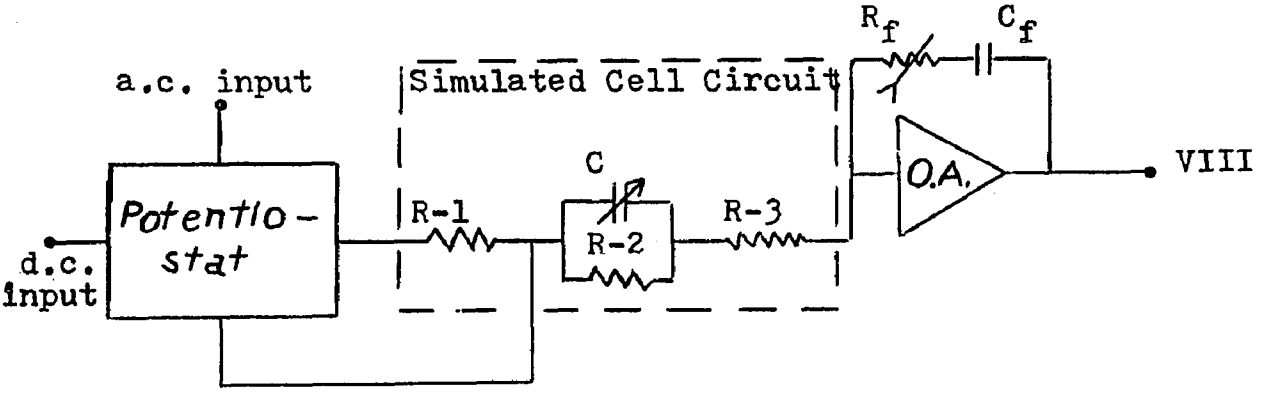

The simulated cell circuit is shown within the dotted line. R-1 is a resistor of about 200 to 300 ohms which simulates solution resistance. R-2 is a 1 megohm resistor which simulated the faradaic d.c. path. C is a standard, variable capacitor which simulates the double-layer capacity and R-3 is a 50 ohm resistor used to simulate resistance which is uncompensated by the potentiostat-due mainly to the resistance of the mercury thread in the capillary of the D.M.E. The calibration was carried out by noting the recorder readout as the standard capacitor was varied over the range of values expected experimentally. In this manner, the need to measure a.c. input and output voltages, the exact value of C_f, the value of δ, etc. is done away with. All that is re-

quired is that the a.c. input voltage be held constant. If δ is very small and/or does not vary significantly, a linear calibration curve will be obtained. If δ varies significantly, a non-linear curve will be obtained. In either case, good compensation for the effect of δ is obtained. As it turned out, the response of the current amplifier was directly proportional to capacity, within experimental error, over the entire range of calibration values at 1 KHz. At 10 KHz there was a definite though slight deviation from linearity which amounted to about three per cent over the entire calibration range.

In practice, the standard variable capacitor consisted of a decade capacitor (General Radio Type 980-A) which could be varied from 0 to 1.0 μf in steps of 0.1 μf and an extra 1.0 μf capacitor (Jensen Type KTTE). These capacitors where checked on a Wayne-Kerr model B-221 Universal Bridge and were found to be within one or two parts per thousand of their nominal values. By suitable arrangement of these capacitors, the range from 0 to 2 μf could be covered in 0.1 μf steps. It was found, however, that for the systems investigated in this thesis a range of from 0.3 to 1.3 μf was sufficient.

The first part of the calibration procedure consisted of setting the full-scale response of the recorder for a definite value of capacity in the simulated circuit. For convenience sake, a value of 1 μf was chosen. When C_{f_2} was used in the current amplifier feedback loop (C_{f_2} = 0.01 uf) an approximate-

ly full-scale response was observed on the recorder. An exactly full-scale response was obtained by slightly adjusting the magnitude of the a.c. input voltage to the potentiostat. The magnitude of this a.c. input voltage was then noted using the rectifier-recorder readout for recording the a.c. output of the current amplifier. For the purpose of precision, it was arranged to have this readout correspond to between ninety-five and one hundred per cent of full scale. This voltage was monitored continuously during both the calibration and the experiment. If necessary, the amplitude was readjusted. Since the oscillator output exhibited a small, long-term drift of about one per cent over one or two hours, the error due to changes in the amplitude of the a.c. input voltage during the course of an experiment was, thus, held to within the reading error of the strip-chart recorder. This error was of the order of two parts per thousand. In experiments at 1 KHz where the response was observed to be directly proportional to capacity, this was all that was necessary for complete calibration. At 10 KHz a complete calibration curve was recorded.

Recalling the section of this thesis on operating points, only responses that ranged from half to full scale were used. Thus, with C_{f_2} in the feedback loop of the current amplifier values of C_d from 0.5 to 1.0 μf could be read. By switching to C_{f_1} ($= C_{f_2}/2$) values of C_d from 1 to 2 μf were covered. Although the method of calibration used here eliminates the need to determine the exact value of the feedback capacitors,

these were checked on the Wayne-Kerr bridge to insure that their ratio was as stated above. Measurement showed that this was the case to within experimental error.

Determination of Flow Rate of Mercury in the D.M.E.

The rate of flow of mercury from the D.M.E. was determined at four different potentials during a run, the total change in flow rate amounting to about one per cent. A calibration curve of flow rate versus potential was drawn from this data and was used to obtain the flow rate at the potential of interest.

To determine the flow rate, mercury was collected for a measured period of time at a given potential. This collected mercury was withdrawn via the teflon stopcock in the bottom of the cell, washed with distilled water and then acetone, dried in a stream of nitrogen and weighed. At least 0.3 g. of mercury was collected during each measurement and since the flow rate was about 1 mg. per second, this involved time periods of about 300 seconds and longer. Since the mercury was weighed to $\pm$ 0.1 mg. and the time was measured to $\pm$ 0.1 second, the accuracy of these measurements was better than one part per thousand.

Data Taking

The data taken for each point consisted of the potential of the D.M.E., the recorder reading, the drop time, τ, and the flow rate of mercury. The potential was set manually by adjusting a potentiometer in the d.c. input of the potentiostat and the flow rate measurement has been described. The

recorder trace of C_d consisted of a continuously rising curve followed by a sharp drop-off as each drop fell. The recorder reading was taken at the top of each curve corresponding to the end of drop life. At each potential ten drops were timed and recorded. The average readout of the ten drops was taken, the range of readings over the ten drops was about five parts per thousand at full scale. The drop time was taken by dividing the time required for the ten drops by 10. This time was measured to ± 0.1 second and since the total time involved was about 50 seconds, the drop times thus measured had a precision of about 2 parts per thousand.

Calculations

For comparison with literature values, C_d must be divided by A, the drop area at the time of measurement. This gives C_d^o, the capacity per unit area, usually expressed in units of microfarads per square centimeter ($\mu f/cm^2$). In order to calculate drop area, the assumption was made that the mercury drop is spherical, an assumption commonly made (7, 28, 31, 35). Then, knowing flow rate, m, and drop time τ, it is a simple matter to show

$$A(cm^2) = 0.8518\ (m\tau)^{2/3} \qquad (36)$$

To obtain C_d^o, C_d is obtained as indicated previously and is divided by the drop area at the end of drop life.

$$C_d^o = \frac{C_d}{(0.8518)\ (m\tau)^{2/3}} \qquad (37)$$

Results and Discussion

Systems Tested and Objectives

The following systems were tested:

1. 1 M KCl
2. 1 mM Zn^{2+} in 1 M KCl
3. 0.1 mM Cd^{2+} in 1 M KCl
4. 0.01 mM Cd^{2+} in 1 M KCl
5. 1 M KNO_3 - 0.1 M KCl
6. 0.1 mM Tl^{+} in 1 M KNO_3 - 0.1 M KCl

All of these systems were tested at two frequencies, viz. 1 and 10 KHz. For systems containing electroactive material, a run was first made on the base electrolyte used in preparing the test solution.

The particular systems listed above were chosen for a number of reasons. Firstly, they all had been reported in the literature (28, 31, 55) thus enabling a comparison to be made between the results of the phase-null method and the literature values. In addition, each system represents a different set of conditions with which to test the method. 1 M KCl and 1 M KNO_3 - 0.1 M KCl represent the ideal case where, due to the absence of electroactive material, the faradaic impedance is infinite and the equivalent cell circuit is represented exactly as a resistance, R_x, and a capacitance, C_d, in series over the entire range of potentials investigated. (See diagram III in section III.) Zn^{2+} in 1 M KCl is representative of systems where the electrode re-

action is rather slow (shall k_{sh} and large θ). According to the ideas discussed in section III of this thesis, this represents a case where $Z_f \gg Z_{Cd}$ holds true even at low frequencies and relatively high concentrations of electroactive material. Cd^{2+} in 1 M KCl, on the other hand, is representative of those systems involving a rapid electrode reaction (large k_{sh} and small θ). Since the k_{sh} for the reaction $Cd^{2+} + 2e^- \rightarrow Cd$ in chloride media is rather large (31, 49, 50), this system represents a worst case for the phase-null method and it was interesting to see, therefore, under what combination of frequency and concentration of Cd^{2+} that the faradaic contribution to the total a.c. cell current could be neglected. The thallium system was interesting from a different point of view. Earlier investigators of the Tl^+/Tl (Hg) electrode reported anomalous behavior for the phase angle of the faradaic impedance (51, 52). Other investigators (53, 54) devised modified forms of the equivalent circuit for the cell impedance in order to explain this phenomenon. In general, it was agreed that specific adsorption of one or both components of the redox couple was the probable cause. However, all of the experimental work involved, in both the discovery of the effect and in the verification of the proposed equivalent circuits, is subject to doubt, due to the fact that the components of the faradaic impedance were obtained using the Randles vector contruction method, in which they inserted the value for the double-layer capacity determined in base

electrolyte alone. Later, Sluyters-Rehbach (55) was able to show by the method described in section II of this thesis that, in fact, the double-layer capacity is enhanced in the presence of thallium. The latter author showed that if C_d determined in the presence of thallium were used, entirely normal results would be obtained for the faradaic phase angle using the unmodified Randles equivalent circuit for the cell. The thallium system, therefore, serves to illustrate the rather large effect on double-layer capacity of specific adsorption of electroactive material, even if the latter is present in low concentration compared to that of the base electrolyte. This emphasizes the need for determination of C_d in the presence of electroactive species.

Experimental Results

1 M KCl Base Electrolyte - Comparison With Literature

The results obtained for 1 M KCl base electrolyte along with literature values are listed in Table I and shown in figure 4 as a function of potential of the D.M.E. versus the SCE.

As can be seen from inspection of figure 4 the phase-null method reproduces the general features of the capacity-potential curve for mercury in 1 M KCl. The minima occuring at about -0.25 and -1.05 volts versus the S.C.E., the so-called "hump" at about -0.4 volts, as well as the two steep sections are all clearly present.

The numerical agreement with the literature values is, in general, very good. Several portions of the curve, however, deserve further consideration. In the region from about -.45 to -.75 volts, where the rate of change of C_d^o is quite large, the original results of Sluyters-Rehbach (listed in Table III) were significantly lower than those of both Barker and Faircloth and the phase-null method. The agreement between the two latter methods, however, is very good over the entire range of potentials. On comparison of the capacity-potential curves, it was observed that while Sluyters-Rehbach's had the same shape and amplitude as the other two, the entire curve appeared to be shifted by about 30 millvolts to more positive potentials. It thus appears that the discrepancy is due to a systematic, constant error in the voltage of the D.M.E. This would certainly explain why the deviations

Figure 4. Capacity-Potential Curves; 1 M KCl-Comparison With Literature

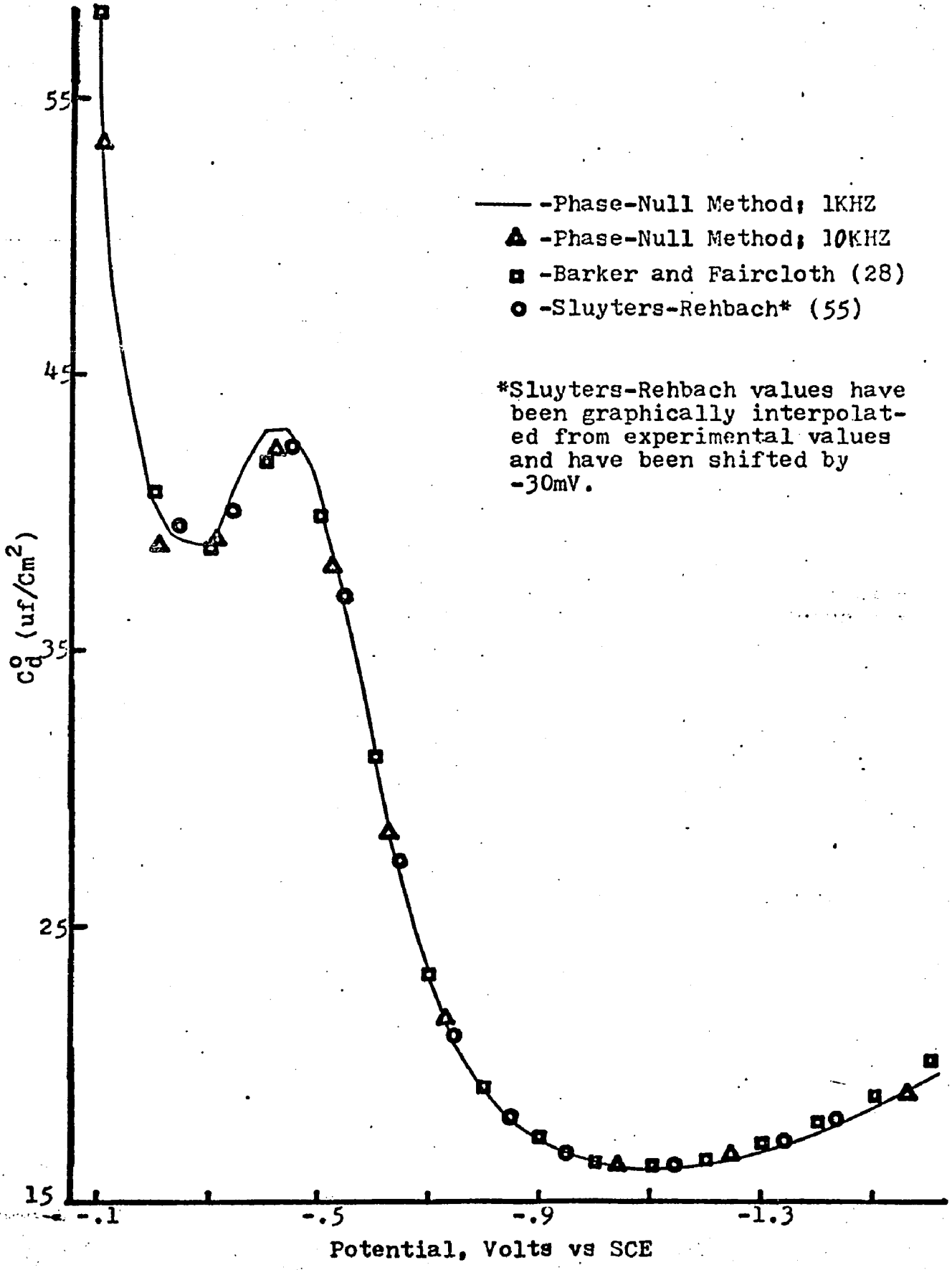

Table I. Differential Double-Layer Capacity of Mercury in 1 M KCl as a Function of Potential at 25° C - Comparison with Literature Values

Potential, Volts vs. S.C.E.	C^o_d ($\mu f/cm^2$) obtained by			
	Barker and Faircloth (28)	Sluyters-Rehbach (55)*	This Study 1 KHz	This Study 10 KHz*
-0.1	58.1	----	57.8	56.7
-0.2	40.7	41.6	40.6	39.5
-0.3	38.7	39.1	39.1	38.6
-0.4	41.8	42.0	42.8	42.1
-0.5	39.9	41.1	40.7	39.6
-0.6	31.2	31.0	31.5	31.0
-0.7	23.3	23.5	23.5	23.2
-0.8	19.2	19.1	19.2	19.2
-0.9	17.4	17.3	17.2	17.2
-1.0	16.5	16.6	16.4	16.3
-1.1	16.4	16.3	16.1	16.1
-1.2	16.6	16.5	16.4	16.3
-1.3	17.2	17.0	16.8	16.8
-1.4	18.0	17.8	17.5	17.5
-1.5	18.9	----	18.3	18.4
-1.6	20.2	----	19.5	19.4

*Obtained by graphical interpolation of experimental values. All Sluyters-Rehbach values have been read at potentials 30 mV more positive than nominal. This corresponds to a shift of the capacity-potential curve along the potential axis by -30 mV.

noted became significant in the potential region where C_d^o is changing most rapidly. For the sake of comparison, the values listed in Table I and shown in figure 4 for Sluyters-Rehbach have all been shifted by -30 mV.

A possible reason for this discrepancy might be that while the potential scale used by Barker and Faircloth and in the present work are experimentally tied to the SCE, that of Sluyters-Rehbach is not. Potentials in the latter work were measured with respect to a mercury pool anode which was assumed to exhibit the potential of the normal calomel electrode (NCE) in 1 molar chloride. To facilitate comparison between the different methods, these potentials were referred to the SCE by calculation. (See section IV of this thesis.) Such a procedure for obtaining electrode potentials could certainly involve a systematic error of the type noted.

Another feature which might be mentioned is that while in the potential region from -0.1 to -1.0 volts there is good agreement with Barker and Faircloth's values, generally about two per cent or better, there is a systematic negative deviation which worsens as the potential becomes more negative than -1.0 volts. At the most negative potential (-1.6 volts) this difference amounts to 3.5 per cent. As of yet, no explanation is advanced for this phenomenon.

Lastly, it will be noted that there is a systematic difference in the phase-null values at 1 and 10 KHz, with the values obtained at the higher frequency being somewhat lower.

This effect, which will be noted in all of the results contained in this thesis, is most pronounced at the most positive potentials where C_d^o is the largest. Grahame (22) first noted this effect and ascribed it to "capillary shielding", that is, the partial blockage of the current lines to the top of the mercury drop by the blunt end of the capillary. Grahame was able to eliminate this effect by the use of specially constructed capillaries with very small outer diameters at the tip and a spherical platinum gauze anode which symmetrically surrounded the mercury drop. More recently, this effect has been ascribed to the so called "capillary response" (56, 57, 58) in which a thin film of solution is postulated as residing between the mercury thread within the capillary and its walls. This solution film may be thought of as an additional impedance in parallel with the electrode impedance. (In the absence of electroactive material, the latter is simply the double-layer impedance.) In any event, the mathematical development of the capillary response theory suggests that the true value of C_d will be obtained upon extrapolation to infinite frequency, whereas Grahame's theory of capillary shielding predicts just the opposite. Experimental evidence has been advanced in support of both theories (58, 59) and the matter is, thus, not settled. A good discussion of this subject is given by M. Sluyters-Rehbach and J. H. Sluyters (60).

1 mM Zn^{2+} in 1 M KCl

The results for the system Zn^{2+} in 1 M KCl are listed in

Figure 5. Capacity-Potential Curves: Zn^{2+} in 1 M KCl at 1 KHz

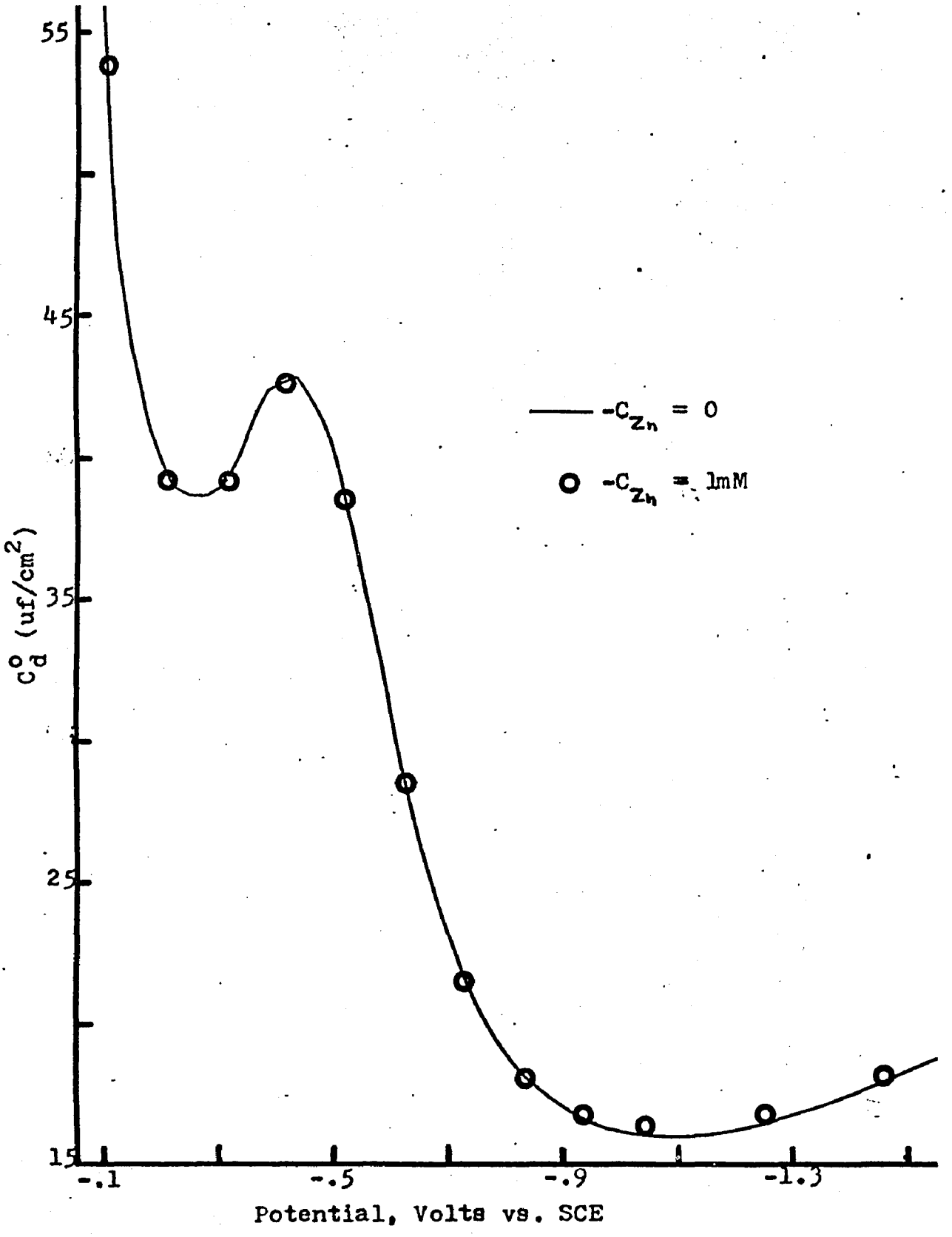

Figure 6. Capacity-Potential Curves; Zn^{2+} in 1 M KCl at 10 KHz

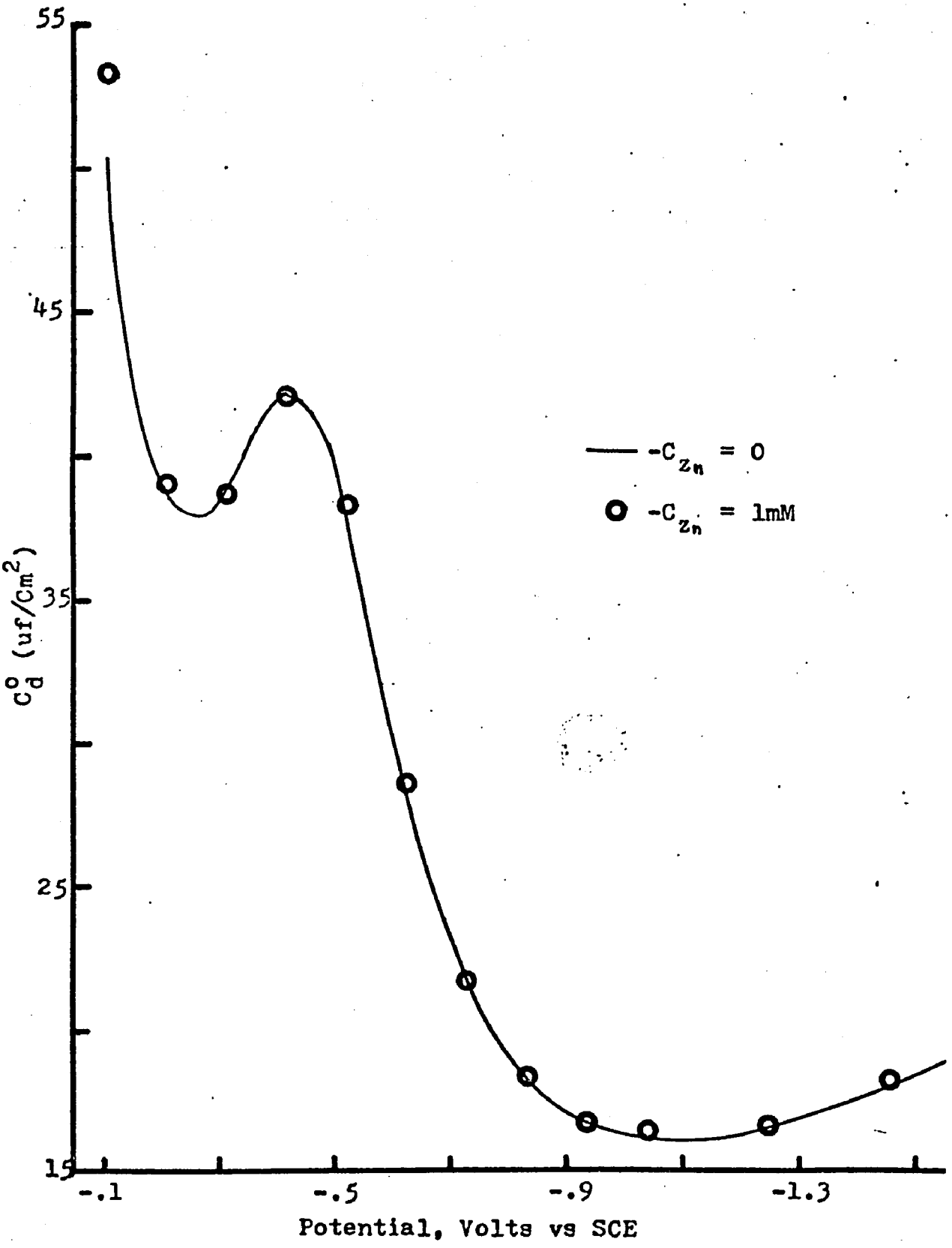

Table II. Differential Double-Layer Capacity of Mercury in 1 M KCl + 1 mM Zn^2 at 1 and 10 KHz

Potential, Volts vs. S.C.E.	C_d^o ($\mu f/cm^2$) at 1 KHz		C_d^o ($\mu f/cm^2$) at 10 KHz	
	No Zn^{2+}	Zn^{2+}	No Zn^{2+}	Zn^{2+}
-0.105	53.9	53.8	50.3	53.3
-0.209	39.3	39.2	38.6	39.0
-0.313	39.2	39.1	38.7	38.7
-0.417	42.8	42.6	42.2	42.1
-0.521	38.5	38.5	37.6	38.3
-0.625	28.5	28.5	28.1	28.6
-0.729	21.6	21.5	21.7	21.7
-0.833	18.2	18.1	18.2	18.4
-0.937	16.6	16.8	16.8	16.8
-1.041	16.1	16.4	16.2	16.5
-1.145	16.1	16.4	16.2	16.5
-1.249	16.4	16.8	16.6	16.7
-1.352	17.1	17.4	17.2	17.4
-1.456	17.9	18.2	18.0	18.3
-1.560	18.9	19.2	19.0	19.4
-1.665	20.5	20.7	20.3	20.8
-1.769	22.4	22.7	22.2	22.8

Figure 7. Capacity-Potential Curves; Zn^{2+} in 1 M KCl- From Data of Sluyters-Rehbach

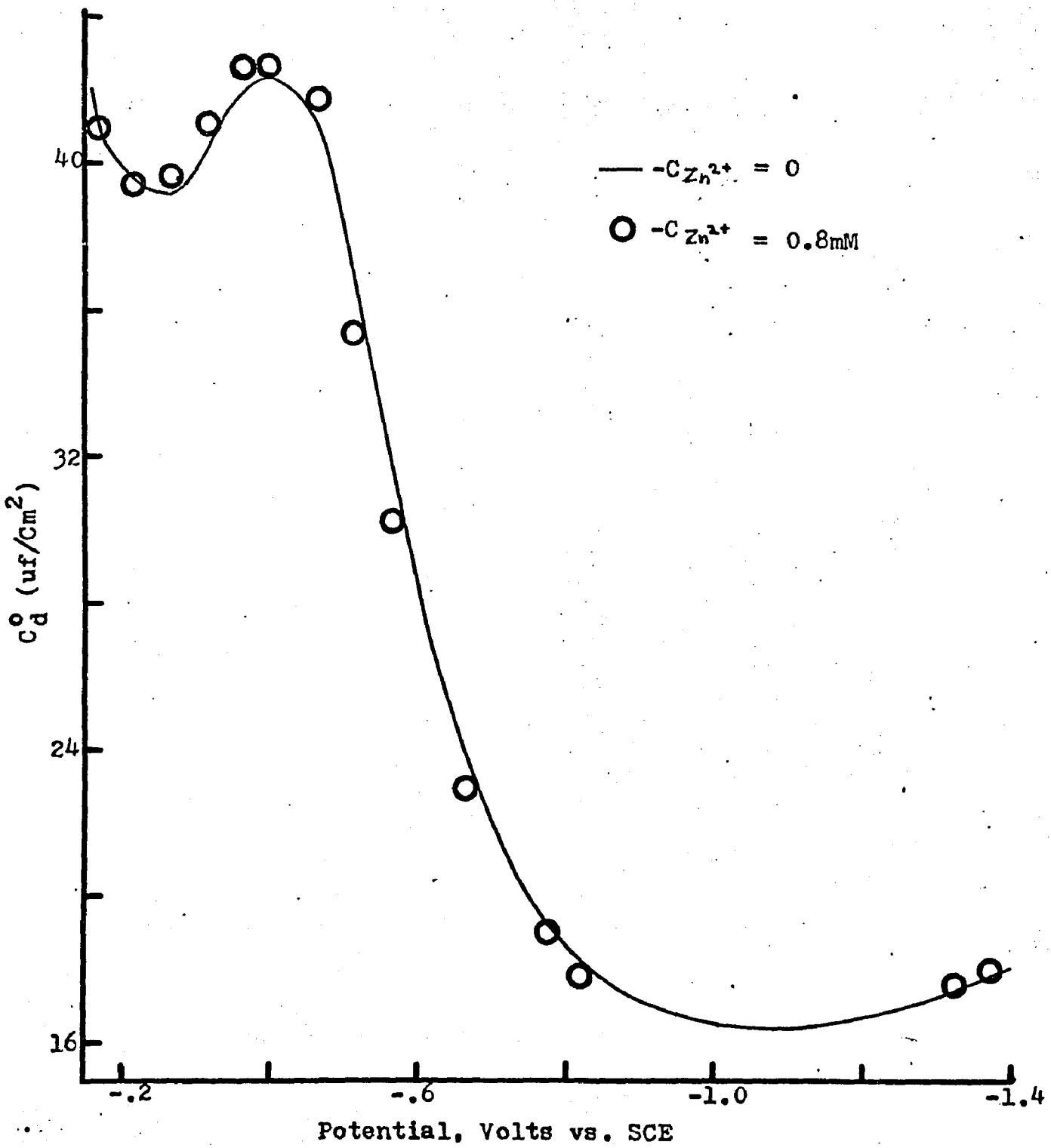

Table III. Differential Double-Layer Capacity of Mercury in 1 M KCl + 0.8 mM Zn^{2} ; Data of Sluyters-Rehbach (55).

Potential, Volts vs. S.C.E.	C_d^o ($\mu f/cm^2$)	
	No Zn^{2+}	Zn^{2+}
-0.167	41.9	40.9
-0.215	39.5	39.4
-0.267	39.1	39.6
-0.316	40.3	41.0
-0.364	41.9	42.6-
-0.395	42.3	42.6+
-0.464	41.3	41.7
-0.513	37.0	35.3
-0.564	31.7	30.2
-0.663	23.9	22.9
-0.773	19.1	19.0
-0.817	18.1	17.8
-0.851	17.6	17.5
-1.322	17.3	17.5
-1.369	17.8	17.9

Table II and shown in figures 5 and 6. The results of Sluyters-Rehbach for this system are listed in Table III and shown in figure 7 for comparison. Sluyters-Rehbach noted that Zn^{2+} does not contribute to the double-layer capacity, as is true for most inorganic cations in the presence of a large excess of base electrolyte. This can be seen by the close agreement of the values for the double-layer capacity in base electrolyte and base electrolyte plus zinc. It will be noted that for potentials more positive than -0.7 volts the agreement of values for double-layer capacity in base electrolyte and base electrolyte plus zinc is significantly better for the phase-null method than that of Sluyters-Rehbach. It will also be noted that even at the half-wave potential for zinc in 1 M KCl, at about -1.0 volts, there is no apparent contribution from faradaic a.c. current even at the lower frequency. As noted before, this is due to the low rate constant for the reaction $Zn^{2+} + 2e^{-} \rightarrow Zn$, which leads to a large value for the charge transfer resistance, θ.

There is one small effect which deserves further consideration. It will be seen from inspection of Table II that there is a small systematic difference between the results for base electrolyte and base electrolyte plus zinc at potentials more negative than -1.0 volt, with the values for base electrolyte falling slightly lower than those for the zinc system. This effect is observed at both frequencies. It does not appear to be due to contribution from faradaic a.c. current, since the effect is not diminished either at potentials well re-

moved from $E_{\frac{1}{2}}$, or at the higher frequency, where in both cases the ratio of a.c. charging current to faradaic a.c. current would be considerably improved. Most likely, this effect has its origin in the high-pass filter which might not be 100% efficient in separating faradaic a.c. and d.c. components of the cell current. The high-pass filter is a device which discriminates between signals on the basis of the difference in their frequencies, passing a greater percentage of a signal at a higher frequency than of one at a lower frequency. Since the faradaic d.c. current has a finite frequency due to the increase in current during the life of a drop, the filter will pass a small percentage of it. This effect is enhanced in the case of the zinc system due to the larger concentration used and to the fact that the d.c. current is largest at the most negative end of the potential scale where the rate of change of the d.c. current with time is also the greatest.

0.1 and 0.01 mM Cd^{2+} in 1 M KCl

The results for the systems 0.1 and 0.01 mM Cd^{2+} in 1 M KCl are listed in tables IV, V and VI and shown, in part, in figure 8. The agreement between values, for base electrolyte and base electrolyte plus cadmium is very good over the entire potential range with the exception of the region of the half-wave potential at about -0.64 volts. As Sluyters-Rehbach has noted, cadmium does not noticeably affect the double-layer capacity in the presence of base electrolyte at concentrations of 4 mM or less. Therefore, this agreement is to be expected.

As has been mentioned before, the reaction $Cd^{2+} + 2e^- \longrightarrow Cd^o$ is very fast in chloride media and provides a worst-case test of the phase-null method. This is especially true in the region of $E_{\frac{1}{2}}$ where the assumption that $Z_f \gg Z_{c_d}$ is poorest. Accordingly, the change in C_d^o due to the presence of Cd^{*2} in this potential region is listed in Table VI and shown in figure 8 as a function of concentration and frequency. According to the predictions in section III of this thesis, the double-layer capacity in the presence of electroactive material should approach that of base electrolyte as frequency.is increased and/or concentration is decreased. (Providing, of course, the electroactive material is not specifically adsorbed.) This is precisely the behavior observed. It is seen that at the lower frequency and higher concentration there is a significant deviation from the capacity measured in base electrolyte. When the frequency is increased, holding concentration constant, the deviation is significantly reduced. At the lower concentration of 0.01 mM the faradaic contribution is almost entirely eliminated even at the lower frequency. The increase in frequency to 10 KHz causes a further, small improvement. The deviation at 10 KHz and 0.01 mM at $E_{\frac{1}{2}}$ amounted to slightly less than three per cent which is almost within the expected experimental precision. Thus, the phase-null method is capable of determining C_d, even in the presence of a fast electrode reaction, provided a high enough frequency and/or low enough concentration is employed.

Figure 8. Change in Capacity versus Potential; Cd^{2+} in 1 M KCl-Effect of Frequency and Concentration

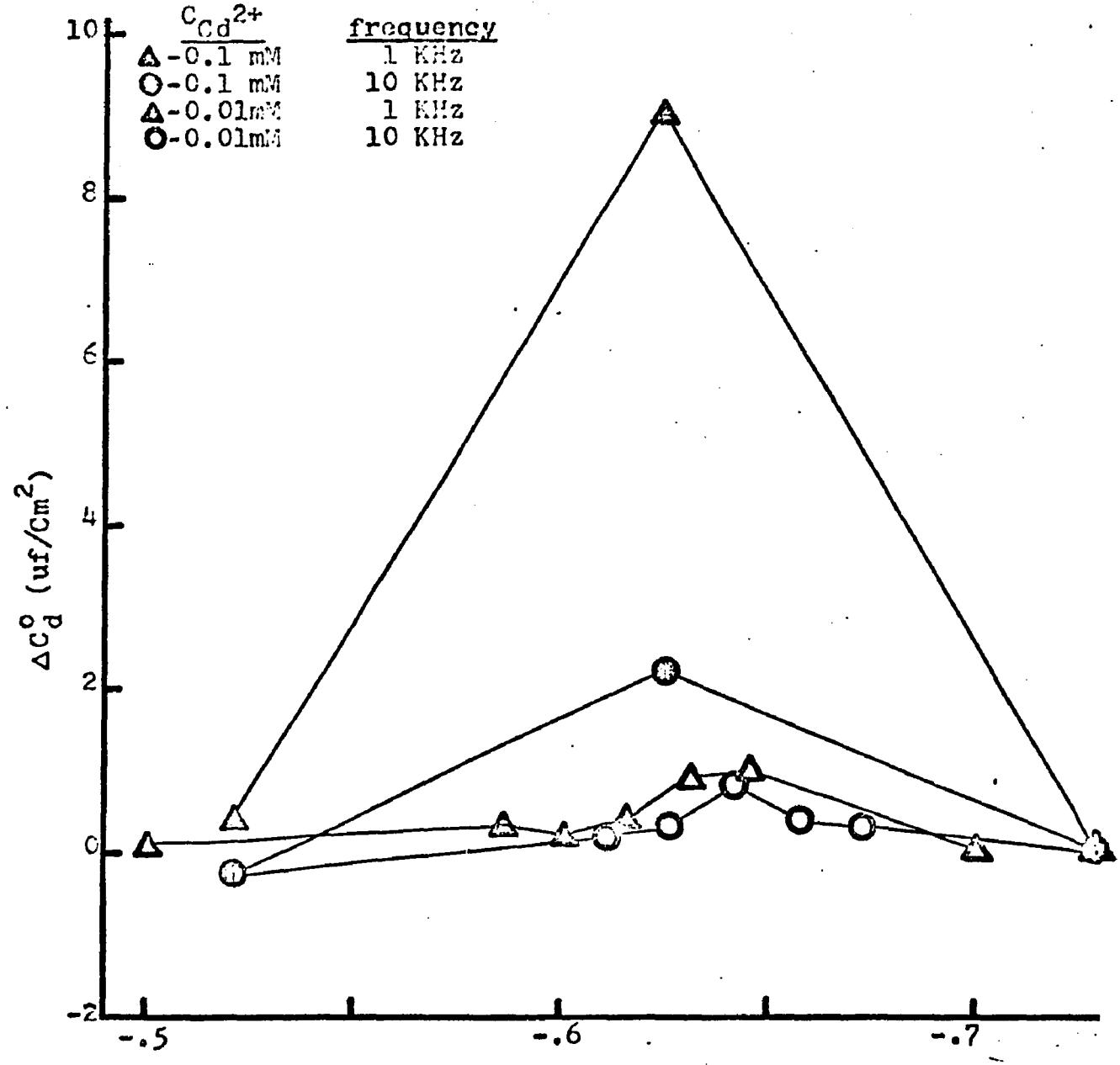

Table IV. Differential Double-Layer Capacity of Mercury in 1 M KCl + 0.1 mM Cd^{2+} at 1 and 10 KHz

Potential, Volts vs. S.C.E.	C_d^o ($\mu f/cm^2$) at 1 KHz		C_d^o ($\mu f/cm^2$) at 10 KHz	
	No Cd^{2+}	Cd^{2+}	No Cd^{2+}	Cd^{2+}
-0.105	54.9	55.2	54.1	54.2
-0.209	39.7	39.8	39.4	39.4
-0.313	39.5	39.5	39.2	39.2
-0.417	43.0	43.1	42.7	42.5
*-0.521	38.8	39.2	38.6	38.3
*-0.625	28.9	37.9	28.8	31.0
*-0.729	21.8	21.9	21.8	21.8
-0.833	18.3	18.3	18.4	18.3
-0.937	16.7	16.9	16.9	16.8
-1.041	16.1	16.3	16.3	16.2
-1.145	16.2	16.2	16.3	16.1
-1.249	16.4	16.6	16.7	16.5
-1.352	17.0	17.2	17.2	17.2
-1.456	17.9	18.0	18.2	18.0
-1.560	19.0	19.1	19.1	19.2
-1.665	20.3	20.4	20.6	20.7
-1.769	22.3	22.4	22.4	22.4

*Data for figure 8 and table VI.

Table V. Differential Double-Layer Capacity of Mercury in 1 M KCl + 0.01 mM Cd^{2+} at 1 and 10 KHz

C_d^o ($\mu f/cm^2$) at					
1 KHz			10 KHz		
Potential, Volts vs. S.C.E.	No Cd^{2+}	Cd^{2+}	Potential, Volts vs. S.C.E.	No Cd^{2+}	Cd^{2+}
-0.1	57.9	57.7	-0.105	52.7	52.8
-0.2	40.6	40.5	-0.209	38.5	39.1
-0.3	39.1	39.1	-0.313	39.0	38.8
-0.4	42.8	42.7	-0.417	42.0	41.6
*-0.5	40.7	40.8	*-0.521	38.0	37.7
*-0.586	32.7	33.0	*-0.611	29.8	30.0
*-0.6	31.5	31.7	*-0.626	28.5	28.8
*-0.616	30.0	30.4	*-0.642	27.0	27.8
*-0.631	28.5	29.4	*-0.658	25.9	26.3
*-0.646	27.3	28.3	*-0.673	24.7	25.0
*-0.7	23.5	23.5	*-0.729	21.7	21.8
-0.8	19.2	19.2	-0.833	18.1	18.3
-0.9	17.2	17.2	-0.937	16.7	16.8
-1.0	16.4	16.3	-1.041	16.1	16.2
-1.1	16.1	16.1	-1.145	16.3	16.2
-1.2	16.4	16.3	-1.249	16.6	17.3
-1.3	16.8	16.7	-1.352	17.1	17.6
-1.4	17.5	17.4	-1.456	17.9	18.3
-1.5	18.3	18.3	-1.560	18.9	19.2
-1.6	19.5	19.5	-1.665	20.2	20.0
-1.7	20.9	20.8	-1.769	22.1	22.2

*Data for figure 8 and table VI.

Table VI. Deviation From Base Electrolyte Double-Layer Capacity Around $E_{\frac{1}{2}}$ - Effect of Frequency and Concentration of Cd^{2+}

Potential, Volts vs. S.C.E.	C_d^o ($\mu f/cm^2$) at 1 KHz	C_d^o ($\mu f/cm^2$) at 10 KHz
	$C_{Cd^{2+}} = 0.1$ mM	
-0.521	+0.4	-0.3
-0.625	+9.0	+2.2
-0.729	+0.1	0
	$C_{Cd^{2+}} = 0.01$ mM	
-0.500	+0.1	---
-0.521	---	-0.3
-0.586	+0.3	---
-0.600	+0.2	---
-0.611	---	+0.2
-0.616	+0.4	---
-0.626	---	+0.3
-0.631	+0.9	---
-0.642	---	+0.8
-0.646	+1.0	---
-0.658	---	+0.4
-0.673	---	+0.3
-0.700	0	---
-0.729	---	+0.1

0.1 mM Tl^+ in 1 M KNO_3 - 0.1 M KCl

A comparison between the results of the phase-null method and those of Sluyters-Rehbach for the systems 1 M KNO_3 - 0.1 M KCl and 1 M KNO_3 - 0.1 M KCl + 0.1 mM Tl+ is listed in Table VII. The results of the phase-null method at 10 KHz for base electrolyte and base electrolyte plus thallium are shown in figure 9. It is seen that, for base electrolyte alone, the results of the phase-null method at both 1 and 10 KHz agree well with Sluyters-Rehbach's values over practically the entire potential range; the only exception occuring at the most positive potentials where the double-layer capacity is changing most rapidly. As discussed previously (see discussion for 1 M KCl), this is probably due to differences in potential.

According to the discussion of this system given at the beginning of this section, Tl^+ is specifically adsorbed at the D.M.E. and, thus, enhances the capacity of the double layer. This behavior is clearly illustrated in figure 9. It is seen that in the region near the half-wave potential for Tl^+ (about -0.49 volts), a noticeable rise in capacity occurs in the presence of Tl^+ which peaks at a potential slightly more negative than $E_{\frac{1}{2}}$. The results of the phase-null method at 10 KHz agree well with those of Sluyters-Rehbach-the change in capacity upon addition of 0.1 mM Tl^+ to base electrolyte being essentially the same for both methods. This behavior is illustrated in figure 10 where the change in capacity upon

Figure 9. Capacity-Potential Curves: Tl^+ in 1 M KNO_3-0.1 M KCl-Phase-Null Method at 10 KHz

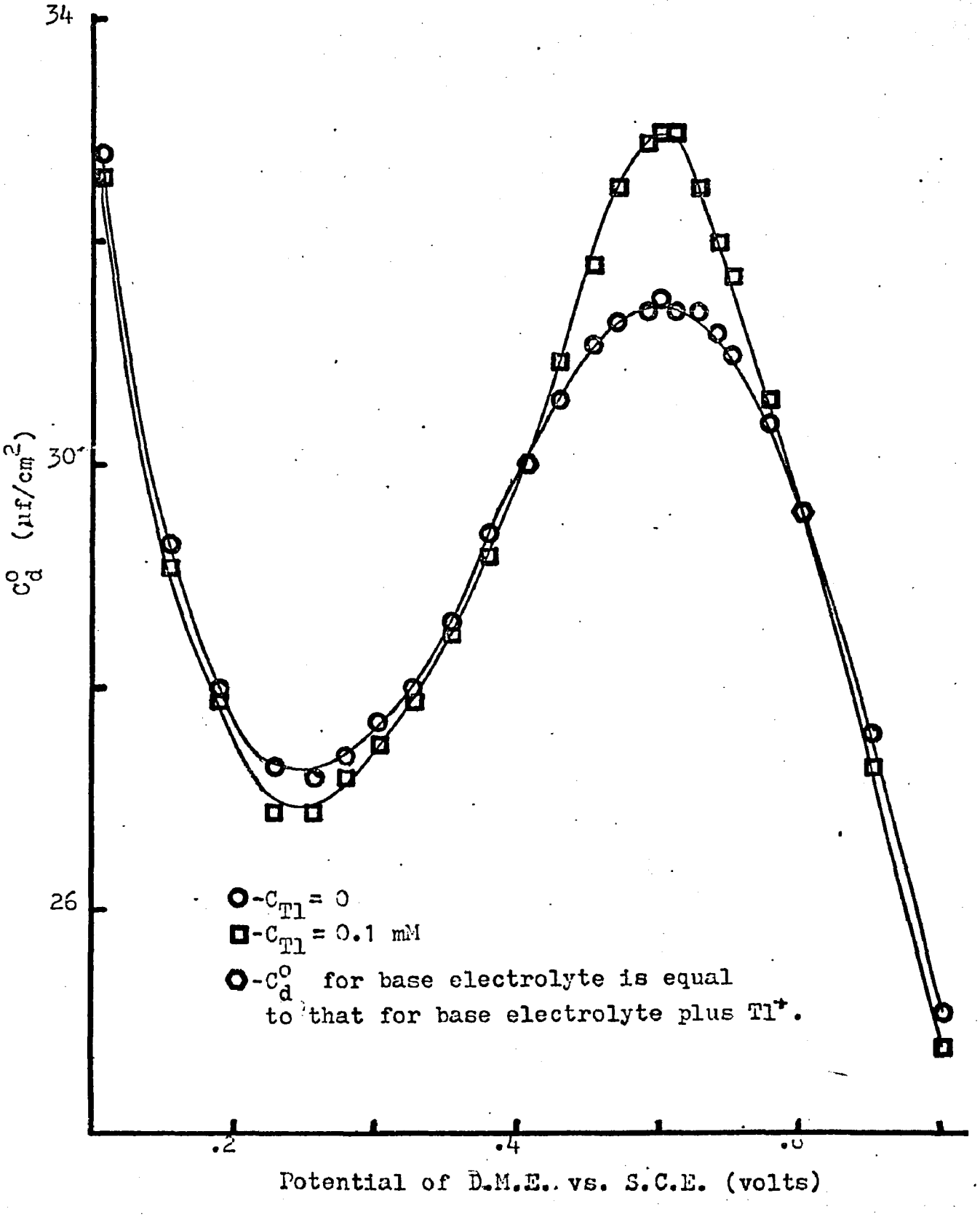

Table VII. Differential Double-Layer Capacity of Mercury in 1 M KNO_3 - 0.1 M KCl + 0.1 mM Tl^+; Phase-Null Method Versus Method of Sluyters-Rehbach (55)

	C_d^o ($\mu f/cm^2$) according to					
	Phase-Null at				Sluyters-Rehbach	
	1 KHz		10 KHz			
Potential, Volts vs. S.C.E.	No Tl^+	Tl^+	No Tl^+	Tl^+	No Tl^+	Tl^+
-0.050	41.7	41.8	40.2	39.8	44.7	45.2
-0.104	33.4	33.6	32.8	32.6	34.9	35.4
-0.153	29.8	29.8	29.3	29.1	30.5	30.7
-0.187	28.3	28.5	28.0	27.9	28.6	28.9
-0.226	27.6	27.7	27.3	26.9	27.6	27.8
-0.253	27.4	27.5	27.2	26.9	27.5	27.7
-0.277	27.5	27.8	27.4	27.2	27.5	27.8
-0.300	27.7	28.0	27.7	27.5	27.8	28.1
-0.325	28.2	28.5	28.0	27.9	28.1	28.6
-0.352	28.8	29.3	28.6	28.5	28.7	28.8
-0.378	29.4	30.2	29.4	29.2	29.4	29.6
-0.404	30.2	31.5	30.0	30.0	30.2	30.4
-0.428	30.8	32.9	30.6	30.9	30.6	31.1
-0.452	31.3	34.8	31.1	31.8	31.1	31.7
-0.469	31.4	36.2	31.3	32.5	31.4	32.2
-0.490	31.8	37.0	31.4	32.9	31.6	32.7
-0.500	31.8	36.5	31.5	33.0	----	33.1
-0.510	31.8	36.1	31.4	33.0	31.7	33.2
-0.526	31.8	34.9	31.4	32.5	31.6	33.0
-0.539	31.6	33.9	31.2	32.0	31.5	32.7
-0.550	31.4	33.2	31.0	31.7	31.3	32.3
-0.577	30.6	31.7	30.4	30.6	30.5	31.3
-0.600	29.9	30.4	29.6	29.6	29.7	30.2
-0.649	27.7	27.9	27.6	27.3	27.5	27.7
-0.700	25.2	25.3	25.1	24.8	25.0	25.3

Figure 10. Change in Capacity versus Potential; Tl^+ in 1 M KNO_3-0.1 M KCl-Phase-Null Method versus Sluyters-Rehbach

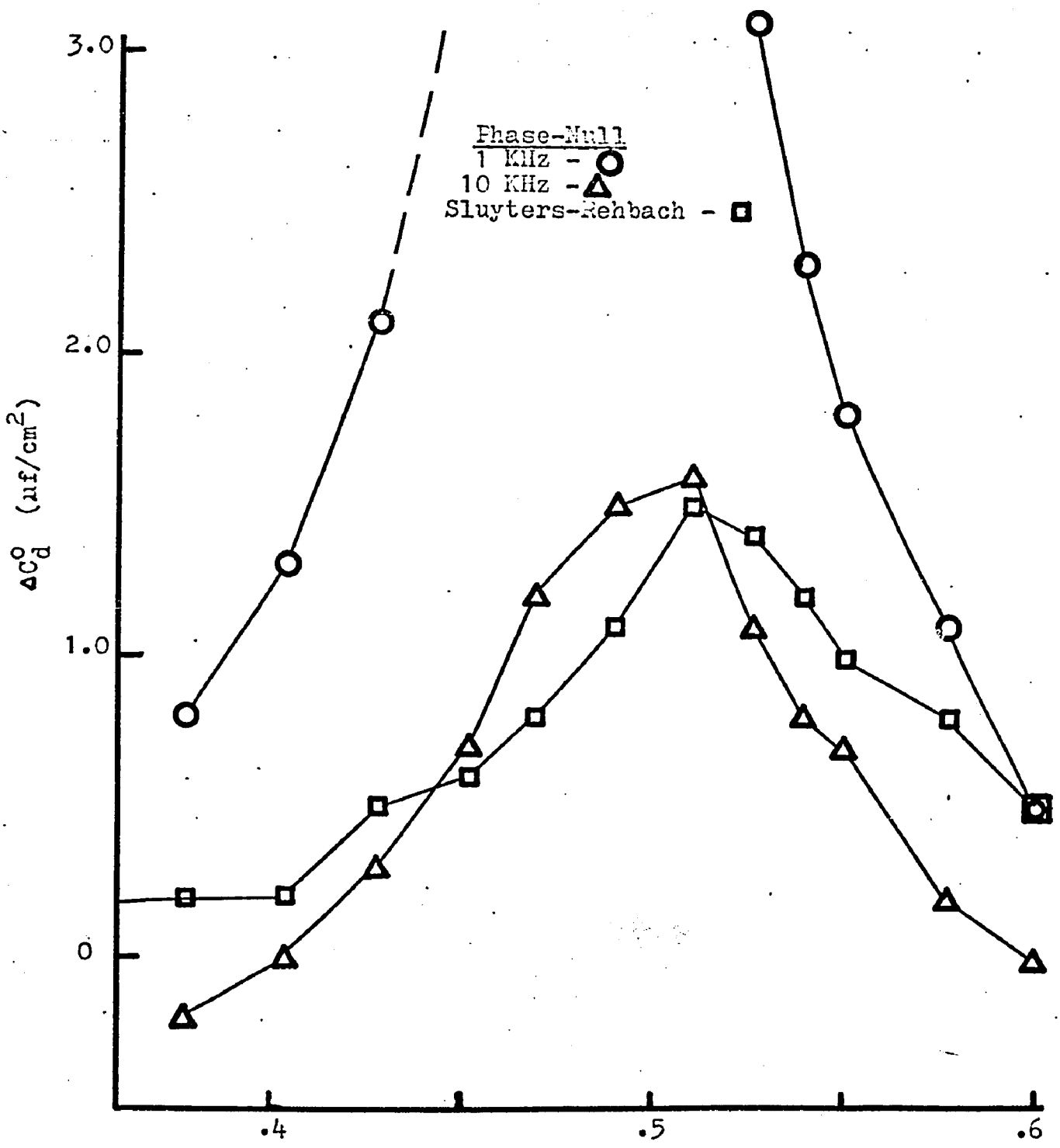

Table VIII. Change in Differential Double-Layer Capacity of Mercury Upon Addition of 0.1 mM Tl^+ to 1 M KNO_3 - 0.1 M KCl; Phase-Null Method Versus Method of Sluyters-Rehbach (55)

Potential of D.M.E. vs. S.C.E. (volts)	C_d^o ($\mu f/cm^2$) according to Phase-Null at 1 KHz	Phase-Null at 10 KHz	Sluyters-Rehbach
-0.104	+0.2	-0.2	+0.5
-0.153	0	-0.2	+0.2
-0.187	+0.2	-0.1	+0.3
-0.226	+0.1	-0.4	+0.2
-0.253	+0.1	-0.3	+0.2
-0.277	+0.3	-0.2	+0.3
-0.300	+0.3	-0.2	+0.3
-0.325	+0.3	-0.1	+0.5
-0.352	+0.5	-0.1	+0.1
-0.378	+0.8	-0.2	+0.2
-0.404	+1.3	0	+0.2
-0.428	+2.1	+0.3	+0.5
-0.452	+3.5	+0.7	+0.6
-0.469	+4.8	+1.2	+0.8
-0.490	+5.2	+1.5	+1.1
-0.500	+4.7	+1.5	+1.5
-0.510	+4.3	+1.6	+1.5
-0.526	+3.1	+1.1	+1.4
-0.539	+2.3	+0.8	+1.2
-0.550	+1.8	+0.7	+1.0
-0.577	+1.1	+0.2	+0.8
-0.600	+0.5	0	+0.5
-0.649	+0.2	-0.3	+0.2
-0.700	+0.1	-0.3	+0.3

addition of Tl^+ to the base electrolyte is shown as a function of potential for both Sluyters-Rehbach's results and those of the phase-null method at 1 and 10 KHz. (See Table VIII for a listing of this data.) It is seen that at 1 KHz the results of the phase-null method are significantly higher than those of Sluyters-Rehbach and the phase-null method at 10 KHz. This is due to the contribution of faradaic a.c. current from the electrode reaction $Tl^+ + e^- \longrightarrow Tl^0$ which has a rather large rate constant in 1 M KNO_3 - 0.1 M KCl (55). Increasing the frequency to 10 KHz eliminates this effect, leading to the observed agreement with the literature values.

Evaluation of Precision

Estimated Precision

The precision of the phase-null method is limited by the precision of the following factors:

1. A. C. input voltage.
2. Drop area.
3. Recorder readout.
4. Potential of the D.M.E.
5. Phase null.

The effect of the precision of items 1, 2 and 3 is constant at all potentials and frequencies, while that of item 4 is a function of the slope of the capacity-potential curve and that of item 5 is a function of the phase angle, α_i, of the equivalent cell circuit which varies with frequency, double-layer capacity and equivalent series resistance.

The error in adjusting and maintaining the a.c. input voltage was essentially due to the usual readout error which amounted to ± 0.2 chart divisions on the recorder. Since it was arranged to have the readout at almost full scale, 100 chart divisions being full scale, the relative precision of this operation was about 2 parts per thousand.

The precision in drop area was limited by precision in flow rate and drop-time measurements, and amounted to about 3 parts per thousand.

The recorder readout precision of 2 parts per thousand at full scale deteriorates to 4 parts per thousand at half scale. For the purposes of estimating the precision of the

readout of C_d the latter value will be used.

Since C_d is a function of potential, the precision with which it can be measured is related to the precision in fixing the potential of the D.M.E. Due to drifts in the potentials of the reference electrodes and uncertainty in readout of the D.M.E. potential, this amounted to ±2 mV as a probable uncertainty and ±3 mV as the worst uncertainty. The effect of this uncertainty upon C_d^o depends on the slope of the capacity-potential curve and, thus, varies over the range of potentials investigated. The relative precision in C_d^o is given by

$$\frac{\Delta C_d^o}{C_d^o} = \frac{(dC_d^o/dE)}{C_d^o} \times \Delta E \qquad (38)$$

where ΔE is the precision of the potential of the D.M.E. In order to evaluate the magnitude of this effect, the slope of the capacity-potential curve in 1 M KCl base electrolyte was measured at three potentials, each potential representing a different slope. These slopes were inserted in Equation (38) and the relative precision of C_d^o was calculated. The results of this calculation are listed in Table IX. For a given uncertainty in potential, it is seen that, in a region of large slope, the error is large and decreases with the slope.

The effect of the uncertainty of 0.3^o in the phase null upon the response of the instrument has already been discussed in section IV of this thesis. (See "Calibration of Electronics")

Table IX. Precision of C_d^o - Effect of Uncertainty in D.C. Potential as a Function of the Slope of the Capacity-Potential Curve

Potential, Volts vs. S.C.E.	$\frac{dC_d^o}{dE}$ ($\mu f/cm^2$ per volt)	$\frac{\Delta C_d^o}{C_d^o} \times 10^3$ probable	worst
-0.105	4×10^2	15	22
-0.417	-2	0.1	0.1
-1.665	-16	2	2

There, it was shown that the fractional change in response due to a phase shift of $\Delta\alpha$ degrees from phase null was given by the term $\sin\Delta\alpha/\tan\alpha_f$ and an upper limit for this quantity was determined. In order to evaluate the actual effect of this term on experimental precision, an estimate must be made of $\tan\alpha_f$ under a given set of experimental conditions. Since α_f and α_i match to better than 0.3°, it is true, to a good approximation, that

$$\tan\alpha_f = \tan\alpha_i \tag{39}$$

Since α_i is given by

$$\tan\alpha_i = -\frac{1}{\omega R_x C_d} \tag{40}$$

we have

$$\tan\alpha_f = -\frac{1}{\omega R_x C_d} \tag{41}$$

Thus, we see that the effect of the phase error signal on experimental precision is a function of frequency, equivalent cell resistance and double-layer capacity. The equivalent cell resistance is due, essentially, to the resistance of the mercury thread in the capillary of the D.M.E. - the effect of solution resistance being practically eliminated by the potentiostat. Thus, this term may be considered constant; a value of 50 ohms was assumed reasonable. However,

since C_d and ω vary, their effect on experimental precision will vary also. The precision will deteriorate as ω and/or C_d increase. The effect of the phase error signal on experimental precision was calculated using values of C_d from 1 M KCl base electrolyte. The results are listed in Table X as a function of frequency and potential. It is seen that the precision deteriorates at higher frequency and at potentials where C_d is large.

In order to calculate the combined effect of the five factors mentioned on the experimental precision, two different calculations were performed. To get a worst case, the effects were added. The probable precision was obtained by taking the square root of the sum of the squares of all the effects. The results of these calculations are listed in Table XI as a function of frequency and potential. It is seen that the biggest effect is at higher frequencies and in steeply sloping sections of the capacity-potential curve.

Observed Precision

The observed precision was evaluated in 1 M KCl at 1 and 10 KHz at the same potentials used in obtaining the estimated precision. Since there was no evidence of contribution to C_d^o from the electroactive species used in 1 M KCl due to specific adsorption and since the potentials were far removed from half-wave potentials, the values for C_d^o obtained with and without electroactive species were used. The observed precision is listed in Table XII. Referring back to

Table X. Precision of C_d^o - Effect of Phase Error Signal as a Function of Frequency and Potential

Potential, Volts vs. S.C.E.	$\frac{\Delta C_d^o}{C_d^o} \times 10^3$ at 1 KHz	$\frac{\Delta C_d^o}{C_d^o} \times 10^3$ at 10 KHz
-0.105	2	19
-0.417	1	16
-1.665	1	6

Table XI. Total Estimated Precision of C_d^o for the Phase-Null Method

	$\frac{\Delta C_d^o}{C_d^o} \times 10^3$ at			
Potential,	1 KHz		10 KHz	
Volts vs. S.C.E.	worst	probable	worst	probable
-0.105	31	21	48	28
-0.417	12	6	26	17
-1.665	12	6	17	8

Table XI, it will be seen that in all cases with the exception of the precision at -1.665 volts and 10 KHz, the standard deviation for observed results is lower than the estimated probable precision. The standard deviation at -1.665 volts and 10 KHz while significantly larger than the estimated probable precision, is still within the estimated worst precision.

Evaluation of Accuracy

In the Absence of Faradaic Current

The accuracy in the absence of faradaic current was limited by the precision as evaluated in the previous section. No phase or gain shifts were noted in the potentiostat at 1 KHz as evidenced by a calibration curve which was linear to within the readout precision of the recorder. At 10 KHz, although slight non-linearity was noticed in the calibration curve, the use of this curve to obtain corrected values for the capacitance readout should eliminate this small effect. Thus, an overall accuracy of about 1% can be claimed in the absence of faradaic current.

In the Presence of Faradaic Current

In the presence of electroactive material, the equivalent cell circuit, from which the gain equation was derived, changes from a simple series connection of R_x and C_d. In this case, the faradaic impedance shunts the double-layer capaci-

Table XII. Observed Precision of the Phase-Null Method

Potential, Volts vs. S.C.E.	$\frac{\Delta C_d^o}{C_d^o} \times 10^3$ Standard Deviation		$\frac{\Delta C_d^o}{C_d^o} \times 10^3$ Range / 2	
	1 KHz	10 KHz	1 KHz	10 KHz
-0.105	13	13	13	14
-0.417	5	9	6	13
-1.665	8	15	10	20

tance. This effect will cause a positive error in C_d for two reasons. The primary effect is an increase in readout due to the increased current. The secondary effect is that shunting of the double layer with the faradaic impedance modifies the phase angle of the equivalent cell circuit to more positive values, since the faradaic impedance has a phase angle of -45° or less while the double-layer impedance has a phase angle of -90°. Since the phase-null servo tracks for phase null, the value of R_f in the presence of faradaic current must increase to match the more positive phase angle of the cell circuit. This will cause an increase in the impedance of the feedback loop of the current amplifier causing a corresponding increase in readout. The magnitude of the error depends on d.c. potential, frequency of the applies a.c. voltage, rate constant for the electrode reaction and concentration of electroactive material.

To evaluate the magnitude of the error caused by the presence of significant faradaic current, we first note that in the absence of faradaic current the readout gives the value for C_d which is the series capacity of the cell circuit. In the presence of faradaic current, the readout will be the <u>equivalent</u> series capacity of the cell. Thus, if it is possible to represent the cell circuit as an equivalent series resistance and capacitance, we can identify the readout as the equivalent series capacitance. The error is the difference between C_d and the equivalent capacity.

Using the Randles equivalent circuit for the cell as a model, the equivalent series capacity, C_{eq}, was solved for in terms of the components of the faradaic impedance and the double-layer impedance (see appendix A-3). The following expression was obtained.

$$C_{eq} = C_d \left[1 + \frac{1 + q}{(2/q)f(p) + 1} \right] \tag{42}$$

Here $q = X_{C_d}/\sigma\omega^{-\frac{1}{2}}$ where X_{C_d} is the capacitive reactance of the double layer, $(1/\omega C_d)$, and $\sigma\omega^{-\frac{1}{2}}$ is the absolute value of the Warburg or diffusion impedance divided by 2; p is given by $\Theta/\sigma\omega^{-\frac{1}{2}}$, where Θ is the activation resistance; $f(p) = 1 + p + p^2/2$. Thus, the relative error in C_d, e, is

$$e = \frac{1 + q}{(2/q)\ f(p) + 1} \tag{43}$$

Thus, the error is a function of p and q. To evaluate the accuracy in the presence of faradaic current, the highest concentration of electroactive material will be found which will give an error no greater than two per cent. This concentration will be expressed as a function of frequency, and rate constant. Worst-case conditions will be assumed. Thus, the d.c. potential will be $E_{\frac{1}{2}}$ and C_d^o will have a minimum value of 15 $\mu f/cm^2$.

Solving the above equation for q and using the approximation $(1-e)^2 \cong 1-2e$ which is good for $e \ll 1$ we get

$$q = \frac{-(1-e)+\sqrt{1+2e(4f(p)-1)}}{2} \qquad (44)$$

Next, q is solved for in terms of concentration and frequency using the previous definition of q in terms of X_{Cd} and $\sigma\omega^{-\frac{1}{2}}$.

$$q = (\omega^{\frac{1}{2}} C_d \sigma)^{-1} \qquad (45)$$

At the half-wave potential it can be shown that (55)

$$\sigma = \frac{4RT}{(nF)^2}\sqrt{(2D)}\, C \qquad (46)$$

where R is the gas constant, T is the absolute temperature, n is the number of electrons involved in the electrode reaction, F is the faraday, D is the diffusion coefficient of the electroactive species and C is the concentration of electroactive species in moles cm^{-3}. Substituting Equation 46 into Equation 45 gives

$$q = \left[\frac{F^2(2D)^{\frac{1}{2}}}{4RT\, C_d^o}\right] \frac{n^2 C}{\omega^{\frac{1}{2}}} \qquad (47)$$

Substituting the following values for the terms in brackets F=96,500, $D=10^{-5}$, R=8.31, T=298, $C_d^o=15 \times 10^{-6}$ gives

$$q = 2.8 \times 10^8 \frac{n^2 C}{\omega^{\frac{1}{2}}} \qquad (48)$$

Setting Equations 48 and 44 for q equal to each other and solving for C in moles per liter gives

$$C(\text{moles/liter}) = \frac{(1.8 \times 10^{-6})\omega^{\frac{1}{2}}}{n^2} \left(\sqrt{1 + 2e(4f(p)-1)} - 1 + e\right) \tag{49a}$$

If $p < 2.5$, the square root can be expanded with an error of less than ten per cent. We then obtain

$$C(\text{moles/liter}) = \frac{(7.2 \times 10^{-6})(\omega^{\frac{1}{2}})(e)f(p)}{n^2} \tag{49b}$$

For a two per cent error, e = 0.02. Substitution of this value of e into Equations 49a and 49b gives respectively

$$C(\text{moles/liter}) = \frac{(4.5 \times 10^{-6})(f^{\frac{1}{2}})}{n^2} \left(0.4\sqrt{6+f(p)} - 0.98\right) \tag{50a}$$

and

$$C(\text{moles/liter}) = \frac{(3.6 \times 10^{-7})(f^{\frac{1}{2}})\, f(p)}{n^2} \tag{50b}$$

where f = frequency ($\omega = 2\pi f$).

The value for p was calculated from (55)

$$p = (\omega D/2)^{\frac{1}{2}}/K_{sh} \tag{51}$$

The maximum value of concentration of electroactive material which would give an error no greater than two per

cent was calculated using either Equation 50a or 50b depending whether $p < 2.5$ or not. The results of these calculations over a wide range of frequency and rate constant are listed in Table XIII.

Referring back to the results for the systems investigated in this thesis, we see that the predictions of Table XIII are substantiated. The rate constant for $Zn^{2+} + 2e^- \rightarrow Zn$ in 1 M KCl has been found by various investigators to be of the order of magnitude of 5×10^{-3} cm sec^{-1} (61, 62, 63, 64). Thus, even at the lower frequency of 1 KHz it was possible to determine C_d^o in the presence of Zn^{2+} at concentrations as high as 1 mM. The reaction $Cd^{2+} + 2e^- \rightarrow C_d$ in 1 M KCl has a rate constant in excess of 1 cm sec^{-1} (31, 49, 50) and, thus, it was necessary to reduce the concentration to 0.01 mM at the higher frequency to obtain accurate results for C_d^o. (Note that since $n = 2$ for the reaction, the values in Table XIII must be divided by four.) The reaction $Tl^+ + e^- \rightarrow Tl^o$ in 1 M KNO_3 - 0.1 M KCl was reported as having a rate constant in excess of 1 cm/sec (55). Thus, using Table XIII one would predict that at the 0.1 mM level a frequency of 10 KHz would be necessary to eliminate significant faradaic contribution to the readout of C_d. This was exactly the behavior observed.

Table XIII. Maximum Values of Concentration of Electroactive Material for Two Per Cent Error in C_d^o at $E_{\frac{1}{2}}$ - Effect of Frequency and Rate Constant

	Concentration in millimoles per liter x n^2					
frequency	k_{sh} (cm/sec)					
(KHz)	∞	10	1	0.1	0.01	0.001
1	0.012	0.012	0.012	0.04	0.8	8
10	0.04	0.04	0.08	0.8	8	--
100	0.12	0.12	0.4	8	--	--
1,000	0.4	0.6	4	--	--	--

Conclusion

Summary

In this thesis, a novel method for the automatic determination of double-layer capacity has been described and tested. The potential of this method for determining double-layer capacity in the presence of an electrode reaction has also been demonstrated.

In section III, it was shown that by proper choice of experimental conditions it is possible to neglect the influence of the faradaic impedance and assume that the equivalent cell circuit consists only of a resistance, R_x, and the double-layer capacity, C_d, in series. If the cell current is fed to an operational amplifier with an R-C circuit in its feedback loop and the feedback resistance is adjusted for phase null, the a.c. gain of the amplifier is equal to the ratio of double-layer capacity to feedback capacity. Thus, the a.c. output voltage of the amplifier is directly proportional to C_d.

In section V various systems were tested and the results compared with literature values. For systems involving only base electrolyte, the agreement with literature values was, in general, very good. It was shown in this section that in the absence of an electrode reaction an absolute accuracy of about 1% can be attained. For systems containing electroactive species the accuracy depended on a number of factors. At potentials removed from $E_{\frac{1}{2}}$ good accuracy was achieved.

In the region of $E_{\frac{1}{2}}$, however, the accuracy was a function of the rate constant, k_{sh}, of the electrode reaction, the frequency of the a.c. voltage and the concentration of electroactive species. From theoretical considerations, the conditions under which the faradaic contribution to $E_{\frac{1}{2}}$ may be neglected were calculated. It was shown that for a slow reaction, typified by the zinc system, the double-layer capacity can be obtained with negligible error even at rather high concentration and low frequency of the applied a.c. voltage. For fast electrode reactions, however, such as the reduction of Cd^{2+} in chloride media or of Tl^{+} in 1 M KNO_3 - 0.1 M KCl, it was shown that the use of higher frequency and/or lower concentration would be necessary to obtain C_d with sufficient accuracy. These predictions were tested and proven experimentally.

The system Tl^{+} in 1 M KNO_3 - 0.1 M KCl demonstrated the effect of even small concentrations of specifically adsorbed material on the double-layer capacity. Even though a large excess of base electrolyte was present, there was a significant enhancement of C_d^o in the presence of a rather small concentration of Tl^{+}. This emphasizes the need for determining C_d^o in the presence of an electrode reaction.

Applications

Compensation for Charging Current

One possible application of the phase-null method is that of compensation for charging current. In d.c. polarography, for example, charging current limits the ultimate sensitivity, preventing determination of electroactive material at concentrations below 10^{-5} M. This is due to the fact that at about this concentration the charging and faradaic currents are of the same order of magnitude. It was shown in section I of this thesis that charging current is directionally proportional to double-layer capacity. Since C_d is automatically determined by the phase-null method, it should be possible by use of appropriate signal-conditioning techniques to use the readout signal of C_d to simulate the charging current electronically and to subtract this from the total cell current. In this manner, it is possible to obtain the true value of the faradaic current automatically. Moreover, at the trace levels of electroactive material where good compensation for charging current becomes important, the accuracy of the phase-null method improves. The accuracy of the method for an application such as this is much better than that indicated in section V of this thesis. There, considerations such as precision of the d.c. potential and drop area were important since C_d^o, the <u>specific</u> differential capacity, was being determined and compared with literature values. These considerations become irrelevant in the present context, the

only basic limitation being the accuracy with which the phase null can be maintained.

It was shown that the relative precision due to imperfect nulling of the phase is given by

$$\frac{\Delta C_d^o}{C_d^o} = \frac{\sin \Delta\alpha}{\tan \alpha_f} \qquad (52)$$

Thus, if the accuracy needs to be improved, there are two approaches which may be employed. One way is to reduce the uncertainty in phase error signal, $\Delta\alpha$, by the use of a more sensitive phase detector. The other approach is to increase the value of α_f. Since α_f tracks the phase angle of the equivalent cell circuit, α_i, α_f can be increased by increasing α_i. The most accessible cell parameter for this purpose is R_x, the equivalent series resistance. If R_x is reduced, α_i will increase since

$$\tan \alpha_i = - \frac{1}{\omega R_x C_d} \qquad (40)$$

R_x is reduced significantly by the use of the potentiostatic circuit described in this thesis, since the effect of electrolyte resistance is almost entirely eliminated. The remaining resistance is due mainly to the resistance of the mercury thread in the D.M.E. and to the iR drop between the reference

electrode and the surface of the D.M.E. Smith has shown (65) that for a.c. signals such as employed in this work, complete compensation for this residual resistance can be obtained by the use of a technique involving positive feedback to the potentiostat. Another approach would be to eliminate the resistance of the mercury thread in the D.M.E. by use of a metal capillary. This would be fairly difficult to accomplish, since the metal surface exposed to the solution would have to be insulated except for the capillary orifice.

It should be possible, using the techniques described here, to obtain C_d with an accuracy of one or two parts per thousand. If the charging current can be compensated with this degree of accuracy, it should be possible to extend the sensitivity by three orders of magnitude. Thus, in the case of d.c. polarography, traces of electroactive material at the 10^{-8} M level should be capable of being determined.

Referring back to the equation for d.c. charging current given in section I of this thesis we have

$$i_c = K_o E^* \frac{dA}{dt} \qquad (11)$$

Thus, compensation for d.c. charging current requires knowledge of E_z - the electrocapillary maximum potential, since $E^* = E - E_z$. This requires a separate experiment for each solution, since E_z is dependent on the nature of the solution and is very sensitive to traces of surface-active impurities.

In addition, i_c is directly proportional to integral capacity, whereas the phase-null method indicates differential capacity. Thus, the experimental realization of compensation for d.c. charging current would involve complications.

A more fruitful approach would involve the application of charging-current compensation to derivative polarography. In derivative polarography, one records the voltage-derivative of d.c. current versus potential. Since the total current is the sum of faradaic and charging current contributions, the derivative of the total current, di_T/dE, is given by

$$\frac{di_T}{dE} = \frac{di_f}{dE} + \frac{di_c}{dE} \qquad (53)$$

where i_f is the faradaic current and i_c is the charging current - both d.c. To obtain compensation for charging current the derivative, di_c/dE, must be simulated electronically and subtracted from the measured, total response, di_T/dE. This is rather easy to accomplish using the phase-null method, since, as it turns out, the charging current response, di_c/dE, is directly proportional to differential capacity - not integral capacity. In addition, knowledge of E_z is unnecessary. To show this, we first differentiate Equation 11 with respect to potential.

$$\frac{di_c}{dE} = \left[K_o + E^* \frac{dK_o}{dE}\right] \frac{dA}{dt} \qquad (54)$$

The term in brackets was shown in section I of this thesis to be the specific differential capacity, C_d^o . (See Equations 16, 17 and 18.) Substitution gives

$$\frac{di_c}{dE} = C_d^o \frac{dA}{dt} \tag{55}$$

Now, $C_d^o = C_d/A$ and $A = kt^{2/3}$ and it is easy to show, therefore, that

$$\frac{di_c}{dE} = \frac{2C_d}{3t} \tag{56}$$

Here t is the time in the life of the drop at which measurement takes place. If a strobe technique is employed for sampling the output, t is constant and the charging current contribution is directly proportional to C_d - the output of the phase-null instrument. Hence, all that is required for compensation of charging current in derivative polarography is appropriate scaling of the phase-null output and subtraction from the measured, total current derivative.

An additional benefit which accrues when a derivative technique is employed is that, as Glickstein et.al. have pointed out (66), the effect of charging current and faradaic current become equal when the concentration of electroactive material is of the order of 10^{-6} M - not 10^{-5} M as in regular polarography. With good compensation for the

charging current response, concentrations down to 10^{-9} M may be accessible. In this regard, it has recently been noted by Meyers and Osteryoung (67) that for the technique of differential pulse polarography (DPP), the d.c. charging current contribution is the limiting factor in trace analytical applications. These authors note that the faradaic and charging current contributions become equal when the concentration of electroactive material is about 10^{-6} M for a two-electron process. In the presence of surfactants, which could be found in a biological sample for instance, the capacitive contribution can become "so pronounced as to make direct analysis impossible" - this for a technique which is noted for its rejection of the charging current contribution! On the contrary, a derivative technique employing the phase-null instrument for compensation of charging current would be unaffected by the presence of surfactants, since the charging current contribution is directly measured in the sample solution and applied to the correction of the total response simultaneously. In the DPP method, on the other hand, the rejection of d.c. charging current is based on the subtraction of total current before a voltage pulse - generally about 100 mV - from the total current measured at a given time delay after the application of the pulse-about 50 msec. Since d.c. charging current is a function of potential and drop area, due to the dependence of double-layer capacity on these parameters, and both of these quantities are different at the

two sampling times employed in the DPP method, an error in d.c. charging current compensation is inherent in this technique.

Electrode Kinetics

The determination of C_d in the presence of an electrode reaction would be of great benefit in the field of electrode kinetics for two reasons. Firstly, since the object of experiments in this field is to obtain information about the components of the faradaic impedance, good compensation for charging current is necessary. This is especially true in the determination of rate constants for rapid electrode reactions where high frequencies must be used, and, thus, large charging currents are encountered. Secondly, the value of C_d in the presence of an electrode reaction would provide information on the behavior of the electroactive species in the double layer. Thus, it could be determined, for example, whether or not specific adsorption played a role in the electrode reaction mechanism.

Analysis of Surfactants

Many surfactants become specifically adsorbed at the D.M.E. over a characteristic range of potentials depending on the nature of the surfactant and the supporting electrolyte. The capacity-potential curves resulting from this adsorption are characterized by two sharp peaks, marking the potentials at which desorption occurs, with a region of depressed double-layer capacity - marking the region of maximum adsorption - in between. The magnitude of this effect

is a function of the surface concentration of surfactant at the D.M.E. This surface concentration is related to the bulk concentration of surfactant through the appropriate adsorption isotherm. Sluyters-Rehbach (55) was able to show, for example, that in the case of the thallium system discussed previously, the increase in capacity due to specific adsorption of Tl^+ was directly proportional to the concentration of Tl^+ in the bulk of the solution. Thus, quantitative analysis of electroinactive surfactants may be possible through analysis of their capacity-potential curves.

Appendix A-1

Derivation of Fundamental Equation for the A. C. Gain of the Current Amplifier At Phase Null

In the configuration shown in diagram IV of Section III, often called the inverting configuration of an operational amplifier, the expression for the magnitude of the a.c. gain, G, is given by

$$G = \frac{e_o}{e_a} = \frac{Z_f}{Z_i} \tag{1}$$

where e_o and e_a are the output and applied voltages respectively and Z_f and Z_i are the feedback and input impedances respectively. From a.c. circuit theory we may write for Z_f and Z_i

$$Z_f = R_f + \frac{1}{j\omega C_f} \tag{2a}$$

$$Z_i = R_x + \frac{1}{j\omega C_d} \tag{2b}$$

Where $j = \sqrt{-1}$, R_f and C_f are the feedback resistance and capacity, while R_x is the equivalent series resistance and C_d is the double-layer capacity. Substituting (2a) and (2b) into (1) we obtain after rearrangement

$$G = \frac{C_d}{C_f} \left[(\omega R_f C_f - j) \; / \; (\omega R_x C_d - j) \right] \tag{3}$$

At phase null α_i, the phase angle of the equivalent cell circuit, is equal to α_f, the phase angle of the feedback circuit. This results in

$$\alpha_i = \tan^{-1} -(\omega R_x C_d)^{-1} = \alpha_f = \tan^{-1} -(\omega R_f C_f)^{-1} \qquad (4)$$

This results in,

$$R_x C_d = R_f C_f \qquad (5)$$

Substituting equation (5) into equation (3) we see that at phase null the numerator and denominator of the term in brackets in equation (3) are equal, giving for G_o - the magnitude of the gain at phase null - the expression

$$G_o = \frac{C_d}{C_f} \qquad (6)$$

Appendix A-2

Derivation of the Complete Equation for A.C. Gain Near Phase Null

The configuration for the current amplifier shown in diagram VI in section IV of this thesis is essentially the same as that referred to in Appendix A-1. Hence, it is still true that

$$G = \frac{Z_f}{Z_i} \tag{1}$$

It may be shown that Z_f may be written as

$$Z_f = \frac{1 + j\omega R_f C_f}{R_s^{-1} + j\omega C_f(1+r)} \tag{2}$$

and that Z_i is given by

$$Z_i = (1 + j\omega R_x C_d) \;/\; j\omega Cd \tag{3}$$

where $r = R_f/R_s$. Substituting equation (3) and equation (2) into equation (1) gives

$$G = \left[(1 + j\omega R_f C_f) \;/\; (1 + j\omega R_x C_d)\right] \left[\frac{j\omega C_d}{R_s^{-1} + j\omega C_f (1+r)}\right] \tag{4}$$

Factoring out $j\omega C_d/j\omega C_f$ from the second term in brackets gives

$$G = \frac{C_d}{C_f}\left[(1+ j\omega R_f C_f)/(1 + j\omega R_x C_d)\right]\left[(j\omega R_s C_f)^{-1} + (1+r)\right]^{-1} \quad (5)$$

Rationalizing the term $\left[1 + j\omega R_f C_f\right]\left[(j\omega R_s C_f)^{-1} + (1+r)\right]^{-1}$ gives

$$G = \frac{C_d}{C_f}\left[\frac{1 + j\left\{(\omega R_s C_f)^{-1} + \omega R_f C_f(1+r)\right\}}{(1 + j\omega R_x C_d)\left\{(\omega R_s C_f)^{-2} + (1+r)^2\right\}}\right] \quad (6)$$

It may be shown from equation (2) that the phase angle of the feedback impedance is given by

$$\alpha_f = \tan^{-1} - \left[(\omega R_s C_f)^{-1} + \omega R_f C_f(1+r)\right]^{-1} \quad (7)$$

Similarly, it may be shown that the phase angle of the equivalent cell circuit is

$$\alpha_i = \tan^{-1} - \left[\omega R_x C_d\right]^{-1} \quad (8)$$

Substituting equation (7) and equation (8) into equation (6) gives

$$G = \frac{C_d}{C_f}\left[\frac{(\tan \alpha_f)^{-1} + j}{(\tan \alpha_i)^{-1} + j}\right] \times A \quad (9)$$

Here $A = \left[(\omega R_s C_f)^{-2} + (1+r)^2\right]^{-1}$. Rationalizing equation (9) gives

$$G = \frac{C_d}{C_f}\left[\frac{(\tan \alpha_i \tan \alpha_f)^{-1}}{1 + (\tan \alpha_i)^{-2}}\left\{1 + \tan \alpha_i \tan \alpha_f + j(\tan \alpha_f - \tan \alpha_i)\right\}\right] \quad (10)$$

Using the following trigonometric identities :

$$\tan a - \tan b = \frac{\sin(a-b)}{\cos a \times \cos b}$$

$$1 + \tan^2 a = (\cos^2 a)^{-1}$$

$$1 + \tan a \tan b = \frac{\tan a - \tan b}{\tan(a-b)} = \frac{\sin(a-b)}{\tan(a-b)} \Big/ \cos a \cos b = \frac{\cos(a-b)}{\cos a \cos b}$$

equation 10 can be simplified to give

$$G = \frac{C_d}{C_f}\left[\frac{\sin \alpha_i}{\sin \alpha_f}\left(\cos \Delta\alpha + j \sin \Delta\alpha\right)\right] \times A \quad (11)$$

Here $\Delta\alpha$ is the phase error or difference in phase angle between the output voltage of the current amplifier and the input voltage to the potentiostat. Experimentally, $\Delta\alpha$ is always less than 1° so that $\cos \Delta\alpha \cong 1$; also, the absolute value of G, $|G|$, is measured, since the <u>rectified</u> output of the current amplifier is measured. Thus, relating equation (11) to experimental conditions we obtain

$$|G| = \frac{C_d}{C_f}\left[\frac{\sin \alpha_i}{\sin \alpha_f}\,(1 + \sin^2 \Delta\alpha)^{\frac{1}{2}}\right] \times A \qquad (12)$$

Since $\Delta\alpha < 1^\circ$, $\sin \Delta\alpha < 0.018$ and neglecting the term $\sin^2 \Delta\alpha$ in parenthesis would lead to an error less than 0.1 parts per thousand. Thus, near phase null, the equation for the gain of the current amplifier is

$$|G| = \frac{C_d}{C_f} \frac{\sin \alpha_i}{\sin \alpha_f} \times A \qquad (13)$$

Since $\alpha_i = \alpha_f + \Delta\alpha$, then $\sin \alpha_i = \sin (\alpha_f + \Delta\alpha)$. Using the identity sin(a+b) = sin a cos b + cos a sin b we obtain

$$|G| = \frac{C_d}{C_f} \left[\cos \Delta\alpha + \frac{\sin \Delta\alpha}{\tan \alpha_f}\right] \times A \qquad (14)$$

Again, since $\Delta\alpha < 1^\circ$, then $\cos \Delta\alpha \approx 1$ and therefore

$$G = \frac{C_d}{C_f} \left[1 + \frac{\sin \Delta\alpha}{\tan \alpha_f}\right] \times A \qquad (15)$$

The expression for A given previously can be simplified. "A" was defined as

$$A = \left[(\omega R_s C_f)^{-2} + (1+r)^2\right]^{-1} \qquad (16)$$

Now the term $(\omega R_s C_f)^{-2} \ll 1$ under all experimental conditions and may be neglected. In addition, r is never greater than 5×10^{-3} and $(1+r)^2 = 1 + 2r$ is a good approximation. Thus, equation (15) can now be written as

$$G = \frac{C_d}{C_f} \left[\frac{1 + (\sin \Delta\alpha / \tan \alpha_f)}{1 + 2r}\right] \qquad (17)$$

Since $\sin \Delta\alpha / \tan \alpha_f$ and 2r are at most 0.02 and 0.01 respectively, equation (17) can be modified further using the approximation $(1 + \gamma)/(1 + \delta) \cong 1 + \gamma - \delta$, if γ and δ are $\ll 1$.

Thus, the final equation for the a.c. gain of the current amplifier near phase null is

$$|G| = \frac{C_d}{C_f}\left[1 + \frac{\sin \Delta\alpha}{\tan \alpha_f} - 2r\right] \qquad (18)$$

Appendix A-3

Derivation of the Expression for the Equivalent Series Capacity in the Presence of Faradaic Current

Referring to diagram II of the equivalent cell circuit in section III of this thesis, we see that Z_f, the faradaic impedance, is given by

$$Z_f = \Theta + W_\sigma \tag{1}$$

where Θ is the charge transfer resistance and W_σ is the Warburg impedance. It may be shown (55) that W_σ may be written as

$$W_\sigma = \sigma \omega^{-\frac{1}{2}} (1-j) \tag{2}$$

Substituting equation (2) into equation (1) we obtain, after some rearrangement,

$$Z_f = A(p+1-j) \tag{3}$$

Here, $A = \sigma \omega^{\frac{1}{2}}$ and $p = \Theta/A$. To evaluate Z_{eq}, the impedance of the equivalent cell circuit, we first note that

$$Z_{eq} = R_x + Z_p \tag{4}$$

where Z_p is the equivalent parallel impedance of C_d and Z_f.

Z_p may be evaluated as follows

$$Z_p = \left[\frac{1}{Z_{C_d}} + \frac{1}{Z_f}\right]^{-1} = \frac{Z_{C_d} \times Z_f}{Z_{C_d} + Z_f} \tag{5}$$

Now $Z_{C_d} = -j\, X_{C_d}$ where $X_{C_d} = 1/\omega C_d$. Inserting this definition of Z_{C_d} into equation (5) and recalling the expression for Z_f in equation (3), we obtain for Z_p

$$Z_p = - \frac{X_{C_d}\left[1 + j\,(1+p)\right]}{(1+p) - j(1+q)} \tag{6}$$

Here $q = X_{C_d}/A$. Rationalizing and rearranging equation (6) gives

$$Z_p = - \frac{X_{C_d}}{(1+p)^2 + (1+q)^2}\left[(1+p)\left\{1+(1+q)\right\}\right] - jX_{C_d}\left[\frac{1+q+(1+p)^2}{(1+p)^2 + (1+q)^2}\right] \tag{7}$$

Recalling equation (4), we can write for Z_{eq}

$$Z_{eq} = R_{eq} - jX_{C_d}\left[\frac{(1+q) + (1+p)^2}{(1+q)^2 + (1+p)^2}\right] \tag{8}$$

Here R_{eq} stands for the terms in equation (8) which are not multiplied by j. From a.c. circuit theory it can be shown that the impedance, Z, for a series combination of a resistance, R, and a capacitance, C is given by

$$Z = R - j X_c \tag{9}$$

where X_c - the capacitive reactance - is $1/\omega C$. Comparing equation (9) and equation (8) we see that the impedance of the equivalent cell circuit, Z_{eq}, is equivalent to a series combination of a resistance and capacitance, R_{eq} and C_{eq}, where $X_{C_{eq}}$ is given by

$$X_{C_{eq}} = X_{C_d}\left[\frac{(1+q) + (1+p)^2}{(1+p)^2 + (1+q)^2}\right] \tag{10}$$

Recalling that $X_C = 1/\omega C$, we get after rearrangement

$$C_{eq} = C_d\left[1 + \frac{1+q}{(2/q)\, f(p)+1}\right] \tag{11}$$

where $f(p) = 1 + p + (p^2/2)$.

Appendix A-4

Specifications of Components

Resistors - All Corning, ½ watt, 1% unless otherwise noted; all values are in ohms with K equal to 1000 and M equal to 1,000,000.

R-1	10, ¼ watt
R-2	1 K
R-3	1 K
R-4	1 K
R-5	1 K, 10 turn potentiometer, wire wound, 0.1%
R-6	3 K
R-7	1 K
R-8	100
R-9	1 M
R-10	Clairex 703L photocell
R-11	200
R-12	200
R-13	100 K
R-14	50, ¼ watt
R-15	1 K
R-16	20 K
R-17	75, ¼ watt
R-18	50 K
R-19	Clairex 703L photocell
R-20	50
R-21	1 K
R-22	75, ¼ watt
R-23	10, ¼ watt
R-24	1 K
R-25	2 K
R-26	2 M
R-27	1 M
R-28	100 K
R-29	2.5 K, linear taper, 1 turn potentiometer
R-30	10 K
R-31	100 K
R-32	1 M
R-33	10 K, linear taper, 1 turn potentiometer
R-34	300
R-35	50, ¼ watt
R-36	100 K
R-37	100 K
R-38	1 M
R-39	1 M
R-40	500 K
R-41	2.2 M
R-42	10 K, 10 turn potentiometer, wire wound, 0.1%

Capacitors - All units are polystyrene and rated 200 volts. All values unless otherwise noted are in microfarads. pf = picofarads

C-1	50 pf
C-2	.005
C-3	.01
C-4	.02
C-5	.01
C-6	.02
C-7	.026
C-8	.1
C-9	.1

Diodes

D-1, D-5	Light emitting diodes. General Electric type SSL-22.
D-2, D-3, D-4	IN-34 AC germanium

Inductor

L-1	1.24 Henry, one side of subouncer audio transformer

Amplifiers - All units are solid state operational amplifiers.

A-1, A-3	Analog Devices type 148 A.
A-2, A-6	Analog Devices type 149 A.
A-4, A-5, A-7, A-8	Analog Devices type 801-C.
A-9	Philbrick type P-2A.

GR Impedance Comparator - General Radio type 1605-A Impedance Comparator.

Bibliography.

1. Mohilner, D.M., The Electrical Double Layer, Part I: Elements of Double-Layer Theory, in "Electroanalytical Chemistry," Vol. 1, Bard, A.J., ed., Marcel Dekker, Inc., New York, 1966.

2. Helmholtz, H.L., Ann. Physik., 89, 211 (1853); ibid 7, 337 (1879); Monatsh Preuss. Akad. Sci., Nov. 1881.

3. Quincke, G., Ann. Physik., 113, 513 (1861).

4. Gouy, G., J. Phys., 9, 457 (1910).

5. Chapman, D.L., Phil. Mag., 25, 475 (1913).

6. Stern, O., Z. Elektrochem., 30, 508 (1924).

7. Grahame, D.C., Chem. Rev., 41, 441 (1947).

8. Randles, J.E.B., Disc. Faraday Soc., 1, 11 (1947).

9. Frumkin, A.N., Z. Physik. Chem., 164, 121 (1933).

10. Smith, D.E., AC Polarography and Related Techniques: Theory and Practice, in "Electroanalytical Chemistry," Vol. 1, Bard, A.J., ed., Marcel Dekker, Inc., New York, 1966.

11. Breyer, B., Bauer, H.H., Alternating Current Polarography and Tensammetry, in "Chemical Analysis," Vol. 13, Elving, P.J. and Kolthoff, I.M., eds., Wiley (Interscience, New York, 1963.

12. Reilly, C.N., Stumm, in "Progress in Polarography," Vol. 1, Zuman, P., and Kolthoff, I.M., eds., Wiley (Interscience), New York, 1962, Chap. 5.

13. Grahame, D.C., Soderberg, B.A., J. Chem. Phys., 22, 449 (1954).

14. Frumkin, A.N., Praskurnin, M.A., Trans. Faraday Soc., 31, 110 (1935).

15. Lippmann, G., Ann. Chim. Physik., 5, 494 (1875); 12, 265 (1877).

16. Overbeek, J.T.H., Irreversible Systems, in "Colloid Science," Vol. 1, Kruyt, H.R., ed., p. 146, Elsevier Publishing Co., Amsterdam-New York, 1952.

17. Lippmann, G., Compt. Rend., 76, 1407 (1873); Pogg. Ann., 149, 561 (1873); J. Phys., 3, 41 (1874).

18. Varley, Phil. Trans., 101, 129 (1871).

19. Frumkin, A.N., Z. Physik. Chem., 103, 55 (1923).

20. Philpot, L. St. J., Phil. Mag., 13, 775 (1932).

21. Ilkovic, D., Coll. Czech. Chem. Commun., 8, 170 (1936).

22. Grahame, D.C., J. Am. Chem. Soc., 63, 1207 (1941).

23. Bowden and Rideal, Proc. Roy. Soc., 120 A, 59 (1928).

24. Erdey-Grúz, T., Vdmer, M., Proc. Roy. Soc., 150 A, 203 (1930).

25. Krüger, Z. Physik. Chem., 45, 1 (1903).

26. Grahame, D.C., J. Am. Chem. Soc., 71, 2975 (1949).

27. Kalvoda, R., Coll. Czech. Chem. Commun., 30, 4280 (1965).

28. Barker, G.C., Faircloth, R.L., The Double-Layer Capacity of Mercury in Contact with Concentrated Electrolyte Solutions, in "Advances in Polarography," Vol. 1, Longmuir, I.S., ed., p. 313, Pergamon Press, London (1960).

29. Brzostowska, M., Dabkowski, J., Minc, S., Rocz. Chem., 43, 2171 (1969); Chem. Abstr., 72, 96009V (1970).

30. Randles, J.E.B., Disc. Faraday Soc., 1, 11 (1947).

31. Sluyters-Rehbach, M., Sluyters, J.H., Rec. Trav. Chim., 82, 525 (1963).

32. De Levie, R., Electrochim. Acta, 10, 395 (1965).

33. Bek, R.Y., Lifshits, A.S., Elektrokhimiya, 3, 748 (1967); Chem. Abstr., 67, 96226K (1967).

34. Britz, D., Bauer, H.H., J. Electroanal. Chem. Interfacial Electrochem., 16.13 (1968).

35. Butler, J.N., Meehan, M.L., J. Phys, Chem., 69, 4051 (1965).

36. Berzins, T., Delahay, P., J. Am. Chem. Soc., 77, 6448 (1955).

37. Delahay, P., J. Phys. Chem., 66, 2204 (1962).

38. Gerischer, H., Vielstich, W., Z. Physik. Chem., N. F., 3, 16 (1954).

39. Kooijman, D.J., J. Electroanal. Chem. Interfacial Electrochem., 18, 81 (1968).

40. Gerischer, H., Krause, M., Z. Phys. Chem. N. F., 10, 264 (1957).

41. Van, Leeuwen, H.P., Sluyters, J.H., J. Electroanal. Chem. Interfacial Electrochem., 39, 25 (1972).

42. Ibid., 39, 233 (1972).

43. Reilly, C.N., J. Chem. Ed., 39, A853, A933 (1962).

44. Booman, G.L., Holbrook, W.B., Anal. Chem., 35, 1793 (1963).

45. Schwarz, W.M., Shain, I., Anal. Chem., 35, 1770 (1963).

46. Applications Manual for Computing Amplifiers, Philbrick Researches, Inc., Dedham, Mass., (1966).

47. Hills and Ives, Nature, 165, 530 (1950).

48. Handbook of Chemistry and Physics, 42 ed., Chemical Rubber Publishing Co., Cleveland, Ohio (1961).

49. Barker, G.C., in "Transactions of the Symposium of Electrode Processes, Philadelphia, 1959," ed., Yeager, E., Wiley, New York (1961).

50. Kooijman, D.J., Sluyters, J.H., Electrochim. Acta, 12, 693, 1579 (1967).

51. Tamamushi, R., Tanaka, N., Z. Physik. Chem. Frankfurt, 28, 158 (1961).

52. Salie, G., Lorenz, W., Z. Physik. Chem. Frankfurt, 29, 408 (1961).

53. Rangarajan, S.K., Dass, K.S.G., J. Electroanal. Chem., 4, 237 (1962).

54. Senda, M., Delahay, P., J. Phys. Chem., 65, 1580 (1961).

55. Sluyters-Rehbach, M., Doctoral Thesis, Utrecht State Univ. (1963).

56. Leikis, D.J., et. al., Russian J. Phys. Chem. (Engl. transl.), 38, 997 (1964).

57. de Levie, R., J. Electroanal. Chem., 9, 117 (1965).

58. Grantham, D.H., Thesis, Iowa State Univ., 1962, Diss. Abstr., 23, 3646 (1963).

59. Schuhmann, D., et, al., J. Chim. Phys., 62, 1214 (1965).

60. Sluyters-Rehbach, M., Sluyters, J.H., Sine Wave Methods in the Study of Electrode Processes, in "Electroanalytical Chemistry," Vol. 4, Bard, A.J., ed., Marcel Dekker, Inc., New York (1970).

61. Randles, J.E.B., Trans. Faraday Soc., 48, 951 (1952).

62. Matsuda, H., Ayabe, Y., Z. Elektrochem., 59, 494 (1955).

63. Tamamushi, R., Tanaka, N., Z. Physik. Chem, N. F., 21, 89 (1950).

64. Kambara, T., Ishii, T., Rev. Polarogr., 9, 30 (1961).

65. Smith, D.E., et. al., Anal. Chem., 40 1424 (1968).

66. Glickstein, J., et. al., An Incremental Method of Derivative Polarography, in "Advances in Polarography," Vol. 1, Longmuir, I.S., ed., p. 183, Perganon Press, New York, (1960).

67. Meyers, D.J., Osteryoung, J., Anal. Chem., 46, 356 (1974).